Chemical Geology 669 (2024) 122365

Contents lists available at ScienceDirect

Chemical Geology

journal homepage: www.elsevier.com/locate/chemgeo

Tracing the orogenic sulfur cycle in the Andes using stable isotope composition of dissolved sulfate in thermal springs

Tyler A. Grambling [a,*], Dennis L. Newell [b], Karen G. Lloyd [c], Coleman D. Hiett [b,d], Heather Upin [b], Peter H. Barry [e], Donato Giovannelli [e,f,g,h,i], J. Maarten de Moor [j,k], Agostina Chiodi [l], Gerdhard L. Jessen [m,n], Jenny M. Blamey [o,p], Anna Szynkiewicz [q,*]

[a] Geology Department, Colorado College, 14 E. Cache la Poudre St., Colorado Springs, CO 80903, USA
[b] Department of Geosciences, Utah State University, 4505 Old Main Hill, Logan, UT 84322, USA
[c] Earth Sciences Department, University of Southern California, 3651 Trousdale Pkway, Los Angeles, CA, 90089, USA
[d] Department of Geosciences, University of Arizona, Tucson 85721, USA
[e] Marine Chemistry and Geochemistry Department, MS# 22, Woods Hole Oceanographic Institution, 266 Woods Hole Road, Woods Hole, MA 02543, USA
[f] Department of Biology, University of Naples Federico II, Ed. 7-1D-22, Monte Sant'Angelo, Naples, Italy
[g] Institute for Marine Biological Resources and Biotechnologies, National Research Council (CNR-IRBIM), Ancona, Italy
[h] Earth-Life Science Institute, Tokyo Institute of Technology, Tokyo, Japan
[i] Department of Marine and Coastal Science, Rutgers University, New Brunswick, NJ, USA
[j] Observatorio Vulcanológico y Sismológico de Costa Rica, Universidad Nacional, Avenida 1, Calle 9 Heredia 86, 3000, Costa Rica
[k] Department of Earth and Planetary Sciences, University of New Mexico, Northrop Hall 141, MSC03 2040, 221 Yale Blvd. NE, Albuquerque, NM, USA
[l] Instituto de Bio y Geosciencias del NOA, Universidad Nacional de Salta, Av. 9 de Julio 14, 4405 Rosario de Lerma, Salta, Argentina
[m] Instituto de Ciencias Marinas y Limnológicas, Universidad Austral de Chile, Independencia 631, Valdivia, Los Rios, Chile
[n] Center for Oceanographic Research COPAS COASTAL, Universidad de Concepción, Concepción, Chile
[o] Fundacion Biociencia, Jose Domingo Cañas 2280, Santiago, Chile
[p] Facultad de Química y Biología, Universidad de Santiago de Chile, Santiago, Chile
[q] Department of Earth and Planetary Sciences, University of Tennessee, 1621 Cumberland Ave, 602 Strong Hall, Knoxville, TN 37996, USA

ARTICLE INFO

Editor: Dr. Don Porcelli

Keywords:
Sulfur isotopes
Oxygen isotopes
Sulfate
Thermal springs
Subduction
Andes

ABSTRACT

The cycling of sulfur (S) to the upper crust and surface via thermal springs at convergent margins has not been explored outside areas with active arc volcanism, even though subduction plays a key role in the Earth's long-term S cycle. To address this knowledge gap, we analyzed stable sulfur and oxygen isotope compositions ($\delta^{34}S$ and $\delta^{18}O$ values) of dissolved sulfate (SO_4^{2-}) in 55 thermal springs from five distinct settings in the Andean orogen. These regions are the Peruvian flat slab and backarc, transition between these two, Argentinian backarc, and Chilean forearc. Although the flat-slab settings had lower SO_4^{2-} concentrations (<2000 mg/L) compared to the steep-slab settings (<12,700 mg/L), there was no significant relationship between isotope composition of SO_4^{2-} and slab geometry. The $\delta^{34}S$ and $\delta^{18}O$ values of SO_4^{2-} varied widely across the studied areas (+0.2 to +23.5 ‰ and − 3.3 to +16.0 ‰, respectively) and reflected the isotope compositions of local bedrock endmembers from dissolution of marine evaporites (+5 to +25 ‰ and + 10 to +20 ‰, respectively) and oxidation of magmatic and/or hydrothermal S and ore sulfide minerals with variable $\delta^{34}S$ (0 to +16 ‰). The $\delta^{18}O$ and $\delta^{2}H$ values of thermal spring water (−18.5 to −3.3 ‰ and − 141.1 to −23.7 ‰, respectively) were consistent with meteoric precipitation, and in most cases decreased with increasing altitude following precipitation in the Andes. Generally, our isotope results do not support the direct transfer of slab-derived S/SO_4^{2-} to thermal springs in the investigated settings. Rather, the $\delta^{34}S$ and $\delta^{18}O$ of SO_4^{2-} in the thermal springs are a sensitive indicator of local water-rock interactions that remobilize bedrock S originating from a complex orogenic cycle reflecting tectonic uplift, erosion, weathering, and exhumation history across the duration of Andean Mountain building.

* Corresponding authors.
E-mail addresses: tgrambling@coloradocollege.edu (T.A. Grambling), dennis.newell@usu.edu (D.L. Newell), lloydk@usc.edu (K.G. Lloyd), chiett@arizona.edu (C.D. Hiett), pbarry@whoi.edu (P.H. Barry), donato.giovannelli@unina.it (D. Giovannelli), joost.demoor@una.cr (J.M. de Moor), gerdhard.jessen@uach.cl (G.L. Jessen), jblamey@bioscience.cl (J.M. Blamey), aszynkie@utk.edu (A. Szynkiewicz).

https://doi.org/10.1016/j.chemgeo.2024.122365
Received 6 January 2024; Received in revised form 9 August 2024; Accepted 27 August 2024
Available online 30 August 2024

1. Introduction

The foundational work establishing mantle-to-surface volatile connections through the continental lithosphere in tectonically active areas has mainly focused on the isotope compositions and fluxes of helium (He) and carbon (C) (e.g., O'Nions and Oxburgh, 1988; Sano and Marty, 1995). These studies recognized that hot springs and other thermal features within volcanically active areas carry He and C from multiple sources including upper mantle, subducting slab and overriding lithosphere. More recent studies on hot springs in the Costa Rican arc and Peruvian Andes have deciphered linkages between deep (e.g. mantle, subducted slab) and crustal (e.g. meteoric water, deep brines, bedrock) volatile sources (Newell et al., 2015; Barry et al., 2019; Scott et al., 2020; Hiett et al., 2021; Upin et al., 2023). In the Peruvian Andes, the mantle-derived C and He in hot springs located above the modern flat slab subduction zone and back arc are likely controlled by widespread hydration of the lithospheric mantle via subduction zone processes (Newell et al., 2015; Hiett et al., 2021, 2022). Further, Barry et al. (2019) Fullerton et al. (2021) suggested that slab-derived C sequestration in the Costa Rica forearc might be also influenced by biological assimilation

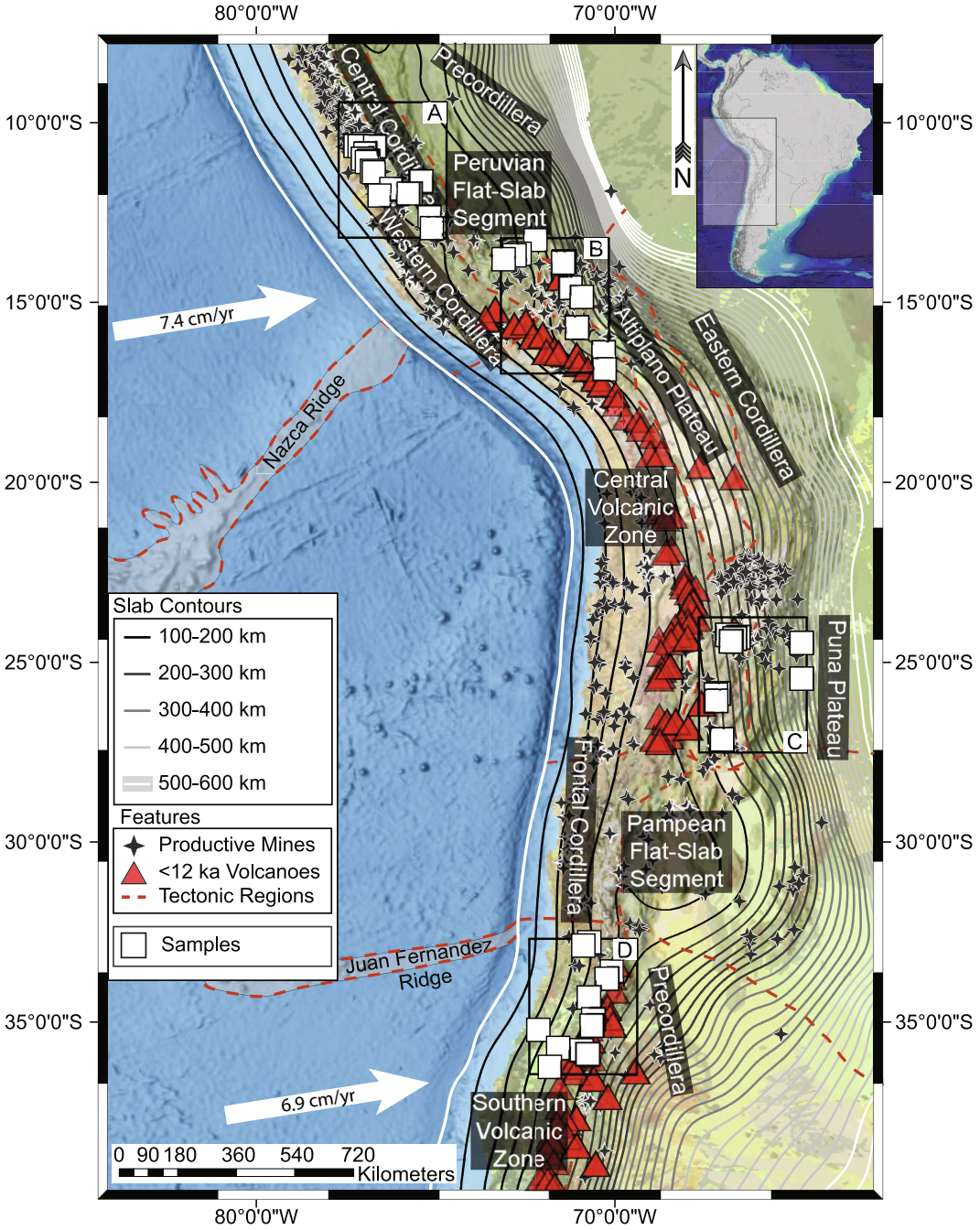

Fig. 1. Vector art file containing a map of the western coast of South America highlighting study areas and sample locations.
(A) Locations of thermal spring sampling points in the central Andes. Grey shaded regions are oceanic ridges and plateaus. Contour lines are depths to slab interface from SLAB 2 (Hayes, 2018) in 20 km intervals, colour changes mark 100 km intervals. Arrows indicate the direction of oceanic plate convergence and velocity with respect to South America. Red triangles are Holocene to modern volcanoes and black stars are historical and/or currently active mines. Dashed lines demarcate tectonic regions or features. (B—D) Locations of detailed geological maps presented in Fig. 3. (For interpretation of the references to colour in this figure legend, the reader is referred to the web version of this article.)

and calcite formation within the continental lithosphere, implying considerable transfer of subducted C into the overriding lithosphere.

Although C and He isotopes have proven reliable indicators of volatile fluxes of these elements into the hot springs and thermal springs across the subduction interface, the sulfur (S) contributions are far less constrained in these settings. This is because the S cycle and budget in subduction zones have been mainly constrained by metamorphic S mineral assemblages in exhumed ancient orogens, modern volcanic degassing and fluid inclusions, devolatilization experiments, geophysical surveys, and numerical models focusing on the mantle wedge, oceanic slab, lower lithosphere, and inactive or active magmatic centers (Hilton et al., 2002; Fischer, 2008; Alt et al., 2012; Tomkins and Evans, 2015; Kagoshima et al., 2015; Bloch et al., 2018; Lee et al., 2018; Rielli et al., 2018; Walters et al., 2020; De Moor et al., 2022;). Whereas these studies have revealed the importance of liberation of aqueous sulfate (SO_4^{2-}) and hydrogen sulfide (H_2S) from the oceanic crust during subduction-related metasomatism, the rapid sequestration of S in the mantle and lower crust seems to be more apparent. This implies that the slab-derived S is unlikely to be directly transported to the hot springs and thermal springs on the surface, in contrast to what is observed with other volatiles. However, elevated SO_4^{2-} concentrations have been reported in thermal waters of subduction settings (Barry et al., 2019; Scott et al., 2020), suggesting additional processes controlling aqueous SO_4^{2-} inputs.

The principle cordilleras of the long lived Andean orogeny (> 150 Ma) (Maloney et al., 2013) from Peru, Chile, and Argentina (Fig. 1) provide an ideal setting to better assess a possible S exchange between subducted oceanic material, subcontinental lithospheric mantle, lower crust, and the surface via thermal groundwater transport. This region covers a wide range of tectonomagmatic settings associated with convergent margins such as: 1) amagmatic, flat-slab subduction zone in central Peru, 2) the transition from shallow to steeply dipping subduction geometry in the northern Altiplano of southern Peru, 3) return of arc magmatic activity and steeply-dipping subduction in southern Peru, 4) magmatically active backarc over the steeply dipping subduction zone in Argentina, and 5) the forearc in Chile (Jordan et al., 1983). We hypothesize that different tectonic regimes, and associated temperature changes across these geologic settings may greatly influence the liberation, migration, and sequestration of slab-, magmatic-, and sediment-derived S into thermal springs. For instance, these differences could result in variability of SO_4^{2-} sources released to thermal waters based on position across the orogen and geodynamic setting.

Therefore, we aim to explore the sources of SO_4^{2-} in thermal springs across the Andes from 10°S to 36°S using sulfur ($\delta^{34}S$) and oxygen ($\delta^{18}O$) isotope compositions. Our overarching goal is to identify the main processes affecting the SO_4^{2-} contributions in thermal waters including the extent of mixing between crustal-, mantle-, and oceanic slab-derived S via thermal springs in the archetype of modern cordilleran orogenies. We report and interpret the new $\delta^{34}S$ and $\delta^{18}O$ values for dissolved SO_4^{2-} from 55 thermal springs in Peru, Argentina, and Chile within the context of different geodynamic settings and regional bedrock geology. These are presented in concert with the oxygen ($\delta^{18}O$) and hydrogen ($\delta^{2}H$) isotope compositions of thermal spring waters to determine their origin and contextualize SO_4^{2-} sources across the central to southern Andes. The selected locations capture the large variability in geodynamic settings across the Andes and are representative of geologic complexity above modern subduction zones. Consequently, our isotope results allow for better determination of SO_4^{2-} sources in the central Andean thermal springs and assessment of possible fluid and S exchange and interactions between deep and shallow subsurface.

2. Geological setting

2.1. Regional tectonic setting

The tectonic evolution of the greater Andes is preserved in the magmatic, sedimentary, and structural records across the studied areas in Peru, Chile, and Argentina (Fig. 1). The western South American margin underwent extension and rifting in the late Jurassic to Cretaceous periods. This led to formation of extensive intracontinental basins, rift-related magmatism, and deposition of the continental margin and marine sediments across the edge of the continent. Conversely, subduction and widespread crustal contraction began forming the Andes in the Cretaceous. This tectonic setting has been maintained since then, resulting in various cycles of slab shallowing, slab rollback, and lithospheric delamination (Decelles et al., 2009; Maloney et al., 2013; Horton, 2018a, 2018b). Local stress variations and changes in slab geometry have resulted in differences in crustal architecture and upper crustal lithology across the Andes. Therefore, variable histories of uplift and exhumation have affected fault penetration depths within the continental lithosphere.

In the central to southern Peruvian Andes, the initial sub-Andean rifting led to crustal thinning between 190 and 140 Ma (Maloney et al., 2013) involving voluminous magmatism (Atherton and Petford, 1996; Maloney et al., 2013). Initiation of subduction in the mid-Cretaceous led to subsequent contraction of the upper and middle crust (Decelles et al., 2009; Scherrenberg et al., 2012; Maloney et al., 2013). This is reflected in thickened supracrustal successions overlaying crystalline basement and intrusive rocks in the Western Cordillera, Altiplano, and Eastern Cordillera. Subduction-related uplift led to exhumation of the Cretaceous-Paleogene plutons to the west of the study areas (Cobbing, 1982; Ramos and Folguera, 2009). The Altiplano region of southern Peru (Figs. 1, 3a) experienced a period of flat-slab subduction in the late Eocene (40–32 Ma) and again in the Oligocene – early Miocene (27–18 Ma). This episode impacted crustal architecture as seen today, leading to broad topographic highs and high elevation plateaus (Ramos and Folguera, 2009; Maloney et al., 2013).

The five study areas we examine here capture thermal springs in a wide range of tectonic regimes that exemplify along-strike variation within the Andean orogeny. The first study area is located to the north of the Altiplano Plateau (Figs. 1, 3b) and lies above the Peruvian flat slab subduction segment that has persisted from ~12 Ma to present age (Hampel, 2002) and is located to the north of the Altiplano Plateau (Figs. 1, 3b). This region transitions to a steeply dipping segment of the subduction zone with a sporadically magmatically active backarc between 13 and 17°S. The second study area is within this transitional zone in a slab dipping beneath the northern edge of the Altiplano Plateau (Figs. 1, 3c). The return to steep subduction is apparent in the third study area, the active Peruvian volcanic arc of southern Peru (Figs. 1, 3c). Overall, these regions in Peru capture the transition from amagmatic shallow to flat subduction zone and to magmatically active, steeply dipping subduction setting (Fig. 2a–c).

The fourth study area encompasses the eastern edge of the Puna plateau and western edge of the Eastern Cordillera in the northern Argentinian Andes and encompasses the southern edge of the Central Volcanic Zone adjacent to the northern edge of the Pampean flat slab (Figs. 1, 3d). This area follows a similar geologic history to the Peruvian backarc and Altiplano, with the only notable difference being the inferred presence of a flat slab from 18 to 12 Ma in the Chilean region versus 35–25 Ma in Peru (Ramos and Folguera, 2009).

The fifth study area is the Chilean Pre-Cordillera, spanning from the coastline to the leading edge of the volcanic arc (Fig. 3d). This segment of the Andes follows deformation patterns established across the orogen, with alternating crustal shortening and extension from 100 to 20 Ma, followed by continuous shortening since ~20 Ma (Parada et al., 1988; Maloney et al., 2013; Horton, 2018b). The studied area experienced a period of flat subduction from 15 to 5 Ma (Ramos and Folguera, 2009; Horton, 2018b) and is within the forearc of the magmatically active Southern Volcanic Zone adjacent to the southern terminus of the Pampean flat slab (Fig. 1).

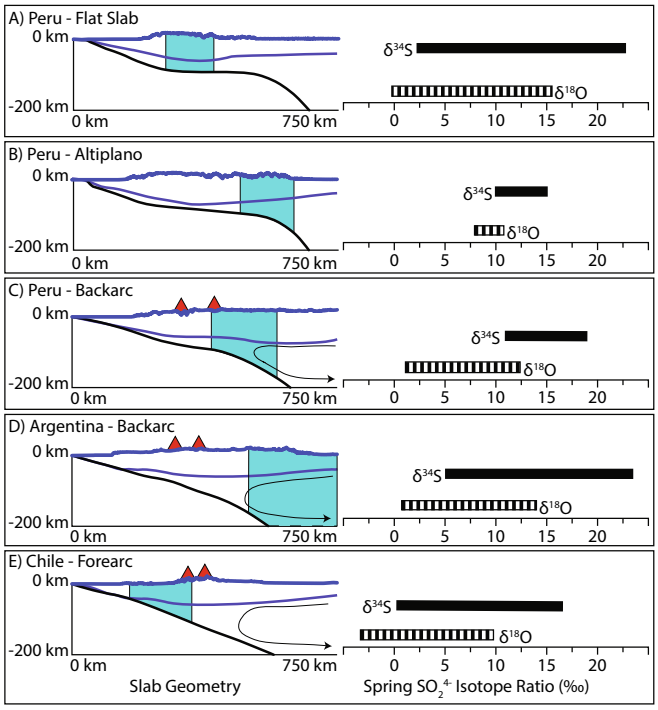

Fig. 2. Vector art file containing topographic and subducted slab profiles for study areas, as well as ranges of $\delta^{34}S$ and $\delta^{18}O$ measured in spring sulfate. Left panels: 750 km × 200 km trench perpendicular topographic profiles from NOAA DEM data, depth to Moho from CRUST 1.0 (Laske et al., 2013), and slab orientation from SLAB 2 (Hayes, 2018) are presented. Blue shaded areas are approximate positions of sampling locations above subducting slab and lithosphere, orange triangles are modern volcanoes, and black arrows show directions of asthenospheric convection. Vertical exaggeration on topographic profiles is 4.5×, no vertical exaggeration beneath datum. Right panels: the ranges of $\delta^{34}S$ (solid lines) and $\delta^{18}O$ (dashed lines) values in the dissolved sulfate of thermal springs sampled in each study area are presented for comparison. (For interpretation of the references to colour in this figure legend, the reader is referred to the web version of this article.)

2.2. Regional geology and ore genesis

The lithology of the studied five Andean regions (Fig. 3) is closely tied to their tectonic evolution. Supracrustal units broadly consist of Jurassic through early Paleogene continental shelf marine sediments overlain by younger continental siliciclastic sequences and volcanic rocks. Paleozoic shelf deposits are present in the Puna Plateau and Eastern Cordillera of Argentina (DeCelles et al., 2011). They comprise Paleozoic through late Mesozoic deep to shallow marine sediments with interbedded chert, limestone, and shale containing sulfate-bearing evaporite deposits and biogenic sulfides, and Mesozoic through Paleogene nearshore and intracontinental sediments with sandstone, conglomerate, and interbedded sandstone and limestone (Coney, 1964; Horton et al., 2001, 2016; DeCelles et al., 2011; Carrapa et al., 2012; Scherrenberg et al., 2012; Horton, 2018a; Sundell et al., 2018).

Plutonic rocks across the study areas vary in age from Cretaceous to Miocene, and in composition from mafic to felsic. Pulses of magmatism across the Andean orogeny occurred in the following time frames: in Peru from 105 to 37 Ma and 13–0 Ma; in the Argentinian backarc and retroarc from 149 to 96 Ma, 77–42 Ma, and 23–0 Ma; and in the Chilean forearc from 191 to 96 Ma, 65–34 Ma, 17–8 Ma, and 5–0 Ma (Coira et al., 1982; Parada et al., 1988; Maloney et al., 2013). As a result, extrusive rocks are widespread on and near the surface, reflecting the history of arc magmatism across all study areas. These units consist of voluminous and widespread Cretaceous through modern bimodal (basaltic to rhyolitic) flows and tuffs overlying deformed sedimentary strata (Cobbing, 1982; Jordan et al., 1983; Parada et al., 1988; Dewey and Lamb, 1992). The sedimentary and volcaniclastic units are overlain and interbedded with unconsolidated modern alluvium and colluvium with occasional playa lake sediments (Petersen et al., 1977; Coutand et al., 2001; Maza et al., 2014; Armijo et al., 2015; Cohen et al., 2015), while modern glaciers are present on higher elevations (Smith et al., 2005; Vimeux et al., 2009; Hoorn et al., 2010).

Since the late Cretaceous, hydrothermal fluid migration associated with magmatism and tectonic burial across the Andes has led to widespread formation of magmatic, epithermal, and sedimentary-hosted sulfur (*S*)-rich ore bodies. Tectonic burial led to diagenetic ore formation involving assimilation of S from the surrounding sedimentary units (e.g., evaporites, biogenic sulfides) and already existing ore deposits (e.g., Flint, 1986). In contrast, ore formation associated with igneous activity involved both addition of new magmatic, oceanic slab and mantle-derived S coupled with some assimilation of S from the country rocks (Fontboté et al., 1990; Basuki et al., 2008; Voute et al., 2019). In the studied areas, these processes led to formation of one of the largest ore deposits on Earth (Flint, 1986; Fontboté et al., 1990; Fontboté and Gorzawski, 1990; Deen et al., 1994; Durieux and Brown, 2007). Generally, magmatic intrusion and devolatilization of magmatic fluids into marine sediments were the primary ore-forming mechanisms in the Andes, whereas burial diagenesis and metamorphic fluid migration led to small, localized ore deposits within sedimentary packages (Deen et al., 1994; Skirrow et al., 2000; Wilson et al., 2003; Catchpole et al., 2015; Voute et al., 2019).

2.3. Thermal springs

Thermal springs in continental convergent settings inform fluid flow paths between the upper crust and the middle to lower crust, as well as volatile mass transfer through the continental lithosphere (Sano and Marty, 1995; Tassi et al., 2010; Scott et al., 2020; Barry et al., 2022). These features are common in the central to southern Andes, and are believed to be sourced by various fluids of shallow and deep origin (e.g., groundwater, magmatic-hydrothermal waters, deep crustal brines) through volcanic conduits and faults (Fontboté et al., 1990; Varekamp et al., 2001; Tassi et al., 2010; Giordano et al., 2013; Newell et al., 2015; Scott et al., 2020; Barry et al., 2022). However, the spring flow paths appear to be heterogeneous and controlled by multiple local factors such as topography and hydraulic head, porosity and permeability of rocks, and fault penetration depths (e.g., Filipovich et al., 2022; Daniele et al., 2022). Although the volatile sources in the Andean thermal springs are less constrained, they are likely sourced from active degassing of magma bodies, upwelling asthenosphere, dehydrating subcontinental mantle lithosphere, and/or deep thermal brines (e.g., Ray et al., 2009; Newell et al., 2015; Scott et al., 2020; Hiett et al., 2021; Lages et al., 2021; Barry et al., 2022).

Previous work has explored the origin of fluids for thermal springs in central to southern Peru. For example, Newell et al. (2015) have shown that up to 25 % of He emitted along the Cordillera Blanca detachment, a deep-seated extensional detachment fault with penetrations depths of >10 km, is likely released by dehydration of the mantle lithosphere and/or upwelling asthenosphere. Conversely, thrust faults south and east of the detachment support shallower (~2–4 km) fluid circulation. While the Peruvian compressional faults do not exhibit characteristics of deep fluid mobility or deep groundwater circulation, fluid flows to depths approaching 8–10 km likely occur along the extensional faults associated with the Cordillera Blanca detachment (Scott et al., 2020). However, the presence of mantle-derived He in several thermal springs in the Cordillera Blanca and the southern Peruvian Altiplano plateau implies that compressional faults may be conduits for deep, lower crustal to mantle-derived volatiles. It is worth noting that similar quantities of the mantle-derived He (~12–14 %) have been estimated in the hydrothermal systems of northern Argentina (Chiodi et al., 2015), thus a similar transfer of the deep volatiles is likely across the studied region (Fig. 1).

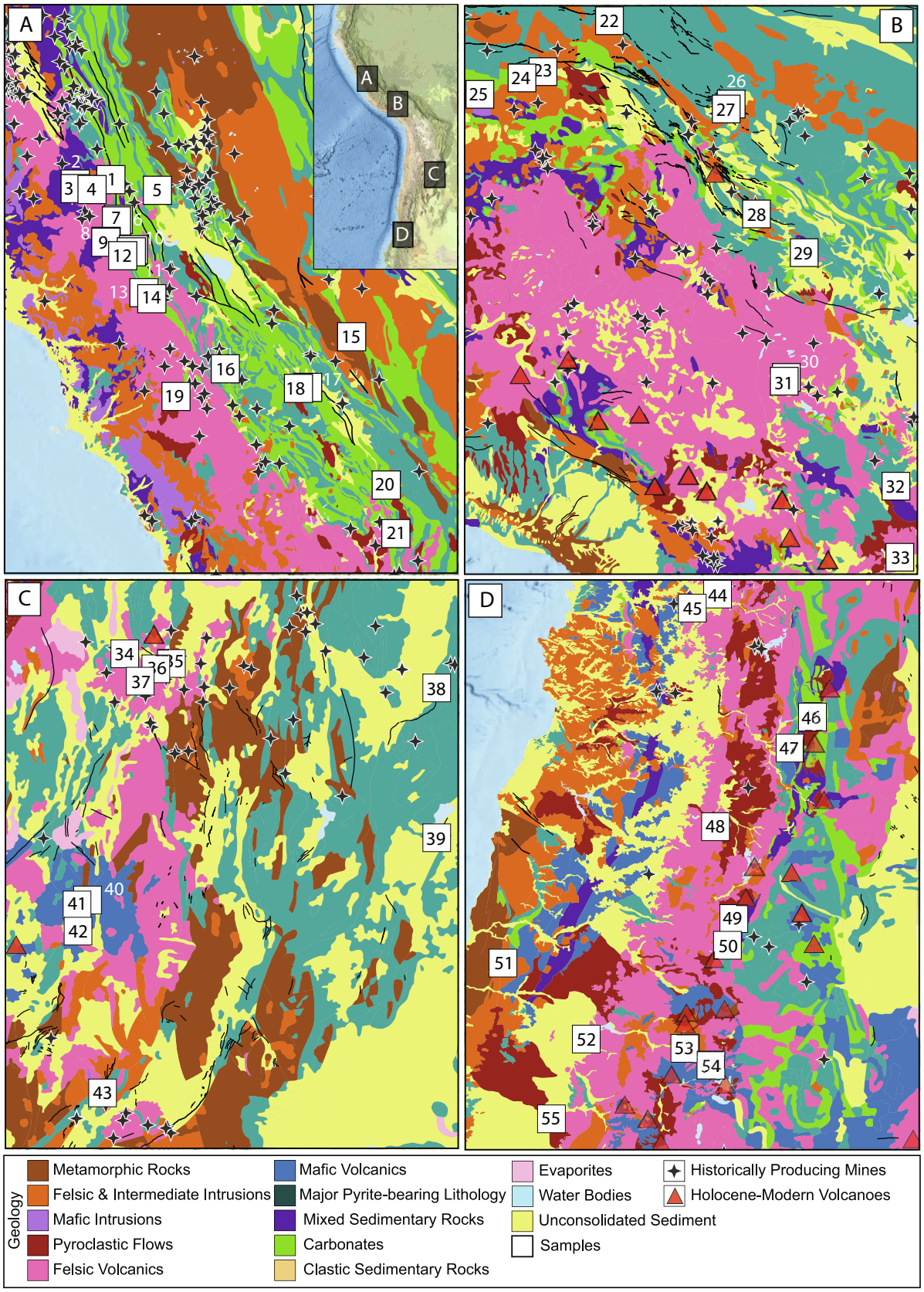

Fig. 3. Vector art file of surficial lithology maps in study area and sample locations.
Geologic maps of each study area highlighting major and sulfur-bearing lithologies (simplified after Hartmann and Moosdorf, 2012) for (A) Central Peru, (B) Southern Peru, (C) Northwest Argentina, and (D) Central Chile. Fault distributions are from Global Earthquake Model Active Faults Database (Styron and Pagani, 2020).

3. Methods

3.1. Field sampling

Peruvian thermal springs occur in settings that are either clearly related to large scale or local faulting or have no direct and observable relationship to faults such as hillside discharges near river and stream networks along the steep canyons. Most of the sampled thermal springs consisted of small features feeding into larger streams and creeks or ponds. The springs sampled at elevations greater than 4000 m above sea level (asl) were usually headwaters for first order streams with visible water inputs from nearby glaciers. Ponded springs (pools) were a result of either engineered or naturally occurring blockages and ranged in size from 1 to 5 m in diameter. The pools were often fed by a single discharge or multiple discharges adjacent to the ponding features. The spring water sample collection was consistent with protocols following Giovannelli et al. (2022) and Hiett et al. (2022). Thus, the fluids were retrieved as close to the main discharge as possible. In instances where multiple discharge points were observed within a single pool, the samples were collected from the point with the highest temperature and/or electrical conductivity.

The Argentinian thermal spring water samples were collected in two different geological settings: 1) high-temperature magmatic geothermal systems within the Neogene-Quaternary volcanic arc in the Puna area and 2) in medium to low temperature geothermal systems associated with deep circulation of meteoric water in the foothills of the Central Andean retroarc-wedge. The Chilean thermal springs were sampled from the forearc of the Southern Volcanic Zone (SVZ) of the Andean Convergent Margin (ACM) at 32–36°S. In these areas, the upwelling of thermal springs is mainly controlled by local faults. Additionally, the Puna thermal springs located at elevations greater than 4000 m asl lacked water inputs from glaciers due to the hyper arid climate. Most of the thermal springs in Argentina and Chile constituted the headwaters for the first order streams and were sampled in similar fashion as in Peru.

In total, 55 thermal springs were sampled over the course of four field seasons during the austral winters of 2018 and 2019 (Peru) and summers of 2019 (Argentina) and 2020 (Chile). 21 samples were collected above the Peruvian flat slab (Locations 1–21), 6 above the slab transition zone in Peru (Locations 22–27), 6 above the Peruvian backarc (Locations 28–33), 10 in the Argentinian backarc (Locations 34–43), and 12 in the Chilean forearc (Locations 44–55) (Figs. 1, 3). Samples were collected in accordance with standard guidelines for groundwater collection (USGS, 2006). Water samples for SO_4^{2-} concentration and isotope analyses were collected into prewashed polyethylene containers. The sampled water was filtered using 0.45 μm nylon membrane filters and stored with no headspace. Measurements of temperature, pH, electrical conductivity (EC) were done in situ prior to water sample collection with an Oakton portable multiparameter meter (Peru) and an YSI multiprobe (Argentina and Chile). The concentration of total dissolved solids (TDS) was calculated based on the EC measurements using the methods described by Rusydi (2018).

3.2. Laboratory analysis

Sulfate (SO_4^{2-}) concentrations were measured using Dionex™ ion chromatography systems at the Utah State University (USU) Water Research Laboratory (Peru samples) and University of Tennessee (UT) Stable Isotope Laboratory (Argentina and Chile samples). Analytical uncertainty during the analysis of SO_4^{2-} concentrations was ±2 mg/L (USU) and ± 5 mg/L (UT). Oxygen and hydrogen isotope compositions ($\delta^{18}O$ and $\delta^{2}H$ values) of thermal water were measured using Cavity Ringdown Spectroscopy (CRDS) on a Los Gatos Research DLT-100 at UT (Argentina and Chile). For Peru samples, these measurements were done using the Thermo Scientific High Temperature Conversion/Elemental Analyzer (TC/EA) and Gasbench II peripheral devices coupled to a Thermo Scientific Delta V Advantage mass spectrometer at USU. High-temperature conversion to H_2 and CO_2 equilibration methods were used to determine $\delta^{2}H$ and $\delta^{18}O$ values, respectively. Results are reported in per mil (‰) relative to Vienna Standard Mean Ocean Water (VSMOW) (Nelson, 2000). Based on standard replicates, analytical precision for $\delta^{18}O$ and $\delta^{2}H$ values was ±0.2 ‰ and ± 1.4 ‰ (UT), and ± 0.1 ‰ and ± 2.0 ‰ (USU), respectively.

Sulfur ($\delta^{34}S$) and oxygen ($\delta^{18}O$) isotope compositions of SO_4^{2-} in all samples were measured at UT. Firstly, water samples were acidified to pH < 3 with a few drops of 12 N HCl to remove bicarbonate/carbonate ions. Secondly, the dissolved SO_4^{2-} was precipitated as $BaSO_4$ by addition of 2 mL of 10 % $BaCl_2$ solution. The precipitated $BaSO_4$ was rinsed three times with DI water before drying in a muffle furnace at 100 °C for 72 h. The $\delta^{34}S$ of $BaSO_4$ was measured using a Costech elemental analyzer (EA) coupled with a Delta Plus XL mass spectrometer. For these analyses, 0.4–0.5 mg $BaSO_4$ was packed with 1–5 mg V_2O_5 in tin capsules to facilitate complete combustion during analysis. The $\delta^{18}O$ of $BaSO_4$ was measured using a Thermo Finnigan TC/EA. For these analyses, 0.15–0.25 mg $BaSO_4$ was loaded into silver capsules with 0.2 mg NaF. Analytical precision was ±0.2 ‰ for $\delta^{34}S$ and ± 0.5 ‰ for $\delta^{18}O$. The $\delta^{34}S$ and $\delta^{18}O$ values are reported in ‰ with respect to Vienna Cañon Diablo Troilite (VCDT) and VSMOW, respectively.

4. Results

All chemical and isotope results for the studied thermal springs from Peru, Chile and Argentina are reported in Supplementary Table 1.

4.1. Water chemistry

The sampled thermal springs had a wide range of temperatures from 8.1 °C to 84 °C (Table S1). The Peruvian segments showed the greatest temperature variation, with the flat slab region spanning from 8.1 °C to 68.4 °C, the transition zone from 27.8 °C to 71 °C, and the backarc from 16.6 °C to 80.5 °C. The highest temperatures were recorded in the Andean backarc region of Argentina (Argentinean backarc from now on), ranging from 27.8 °C to 84.0 °C. Springs in the Chilean region of the Andean forearc (Chilean forearc from now on) ranged from 19.6 °C to 68.4 °C. The thermal springs had water pH ranging from 5.8 to 10.3 (Fig. 4a). Neutral to acidic conditions were prevalent in the thermal springs of Peruvian flat slab (5.8–7.5) and slab transition zone (6.0–6.8), while acidic to basic conditions were present in both the Peruvian and Argentine backarc (6.0–6.2 and 6.3–9.1, respectively). The Chilean forearc spanned the widest pH range of 5.9 to 10.3. Generally, there was no clear relationship between pH and bedrock composition. The TDS of thermal springs varied significantly across the studied areas, from 216 mg/L to 66,822 mg/L (Fig. 4b). For instance, the TDS of springs in the Peruvian flat slab ranged from 216 mg/L to 7127 mg/L, the slab transition from 2090 mg/L to 50,093 mg/L, and the backarc spanned from 2924 mg/L to 12,209 mg/L. The springs of Argentinian backarc and Chilean forearc had similar TDS ranging from 858 to 66,822 mg/L and 606 to 65,600 mg/L, respectively.

4.2. Isotope composition of water

The $\delta^{18}O$ and $\delta^{2}H$ values of thermal springs across the central Andes ranged from −18.5 ‰ to −3.3 ‰ and − 144.1 ‰ to −23.7 ‰, respectively, and were aligned closely with the Global Meteoric Water Line (GMWL) (Fig. 5). Only three water samples from the backarc in Peru and Argentina were considerably enriched in ^{18}O (higher $\delta^{18}O$ values in Locations 27, 33, 34) and consistent with water-rock isotope exchange at elevated temperature and/or evaporation. Most thermal springs showed clear increases of $\delta^{18}O$ and $\delta^{2}H$ values with decreasing altitude (Fig. 6a and b). A few exceptions were the thermal springs with higher $\delta^{18}O$ and $\delta^{2}H$ values in locations 34 and 40–42 (Argentina) near active volcanic centers.

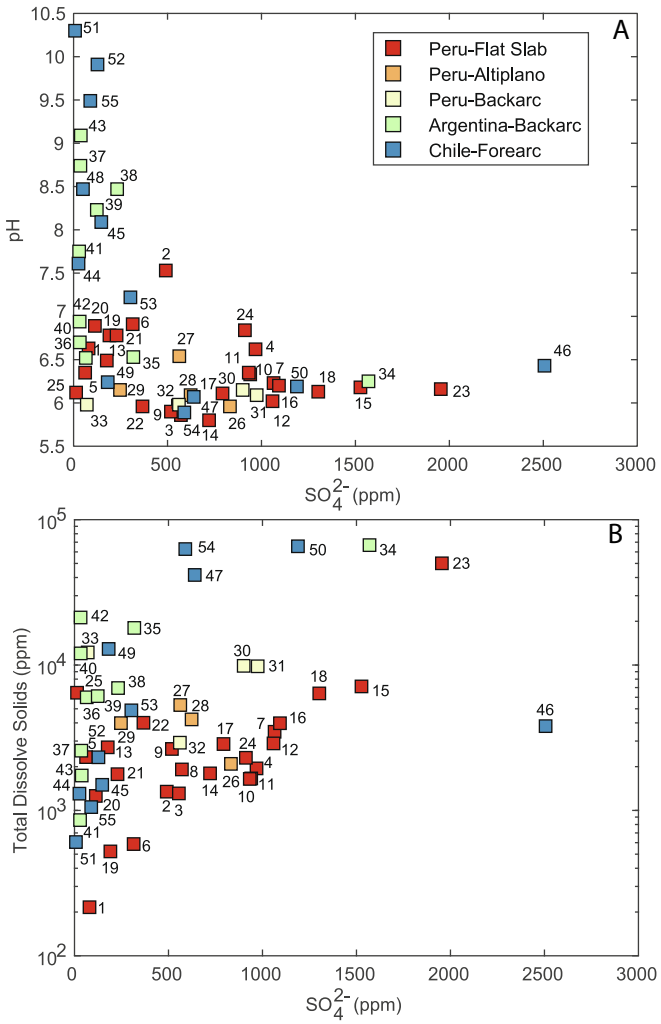

Fig. 4. Vector art file containing a plot of sulfate concentrations vs pH and sulfate concentrations vs total dissolved solids.
Variations of sulfate concentration relative to pH (A) and total dissolved solids (B) in the Andean thermal springs. The alkaline springs with lower sulfate concentrations were usually associated with volcanic, plutonic, and sedimentary bedrock and the acidic springs with higher sulfate concentrations were near surface mining operations and large ore deposits. The springs associated with mining, ore deposits, and evaporites tended to have high TDS and sulfate concentrations, while volcanic/igneous bedrock associated springs had variable TDS, but low sulfate concentrations. Numbers refer to locations of sampling sites presented in Fig. 3.

4.3. Isotope composition of dissolved sulfate (SO_4^{2-})

The $\delta^{34}S$ and $\delta^{18}O$ values of dissolved SO_4^{2-} in thermal springs varied widely from +0.2 ‰ to +23.5 ‰ and − 3.3 ‰ to +16.0 ‰, respectively (Fig. 6). The smallest variation of $\delta^{34}S$ and $\delta^{18}O$ was measured in the Peruvian slab transition (+9.9 ‰ to +15.1 ‰ and + 7.9 ‰ to +10.8 ‰, respectively). Conversely, larger variations of $\delta^{34}S$ and $\delta^{18}O$ were observed in the Peruvian flat slab (+2.2 ‰ to +22.8 ‰ and − 0.5 ‰ to +16.0 ‰), Peruvian backarc (+10.9 ‰ to +19.0 ‰ and + 1.1 ‰ to +10.8 ‰), Argentine backarc (+5.0 ‰ to +23.5 ‰ and + 0.7 ‰ to +14.0 ‰), and Chilean forearc (+0.2 ‰ to +16.6 ‰ and − 3.3 ‰ to +9.9 ‰). Generally, lower $\delta^{34}S$ and $\delta^{18}O$ values of thermal springs were more common in areas with magmatic and ore sulfide deposits and higher values in areas with marine evaporites in the bedrock. In most cases, higher TDS was correlated with higher $\delta^{34}S$ values, and the abundance of sedimentary rock formations exposed at the surface (Fig. 7).

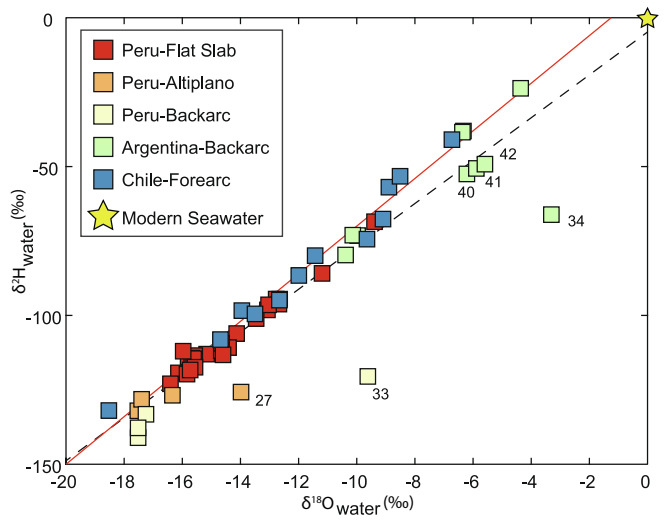

Fig. 5. Vector art file containing plot of $\delta^{18}O$ vs δ^2H for Andean thermal springs.
Variation of $\delta^{18}O$ and δ^2H values in the studied thermal spring water. Solid (red) line indicates Global Meteoric Water Line (Slope = 8.0; Craig, 1961). Dashed (Black) line indicates Local Meteoric Water Line (Slope = 7.1). Numbers refer to locations presented in Fig. 3. (For interpretation of the references to colour in this figure legend, the reader is referred to the web version of this article.)

5. Discussion

5.1. Assessment of slab-derived sulfur in the Central Andes

Sulfur cycling in deep subduction zones have been assessed by numerical simulations (Tomkins and Evans, 2015; Walters et al., 2020) and field-based studies focused on the exhumed rocks (blueschists, peridotites, ophiolites, etc.) of the lower crust, mantle wedge, and mélange zones that formed in steeply dipping subduction zones during past orogenic activities (Tomkins and Evans, 2015; Lee et al., 2018; Rielli et al., 2018; Walters et al., 2019). These studies have suggested that S is released from the subducting oceanic slab by three main processes: 1) thermochemical breakdown of sulfate and sulfide minerals during metamorphism of the slab; 2) metasomatic reactions during serpentinization in the mantle wedge resulting from dehydration of the subducting slab; and 3) compaction and heating that releases pore-water and sediment-bound sulfate from the uppermost oceanic crust. Once liberated, S produced by the first two mechanisms is either sequestered in the mantle wedge or lower continental lithosphere by metamorphic reactions (Tomkins and Evans, 2015; Lee et al., 2018: Rielli et al., 2018; Walters et al., 2019) or incorporated into the arc magmas. The latter leads to formation of magmatic sulfide minerals, often as S-rich ores, and/or S degassing via volcanic conduits (Tomkins and Evans, 2015; Rielli et al., 2018; Walters et al., 2019; de Moor et al., 2022). However, the fate of pore-water and sediment-bound sulfate is still debated in the deep (steep-slab) subduction settings (Lee et al., 2018). Conversely, in the absence of convecting asthenosphere between the oceanic and continental plates, the oceanic slab is subjected to lower pressures and temperatures during shallow subduction while it under rides the continental plate at depths of 70–100 km (Ramos and Folguera, 2009; Manea and Manea, 2011). Consequently, questions remain about the releases of subducted S in flat slab settings and subsequent formation of sulfate (SO_4^{2-})-rich thermal water/fluids. In our study, the examined thermal springs in the flat-slab setting showed smaller ranges of SO_4^{2-} concentrations (61 to 1954 mg/L) compared to the steep-slab settings (4 to 12,698 mg/L; Suppl. Table 1; Fig. 4). This suggests that different processes may contribute to the S budget in these settings.

Pore-water SO_4^{2-} and biogenic H_2S/sulfide minerals originating from

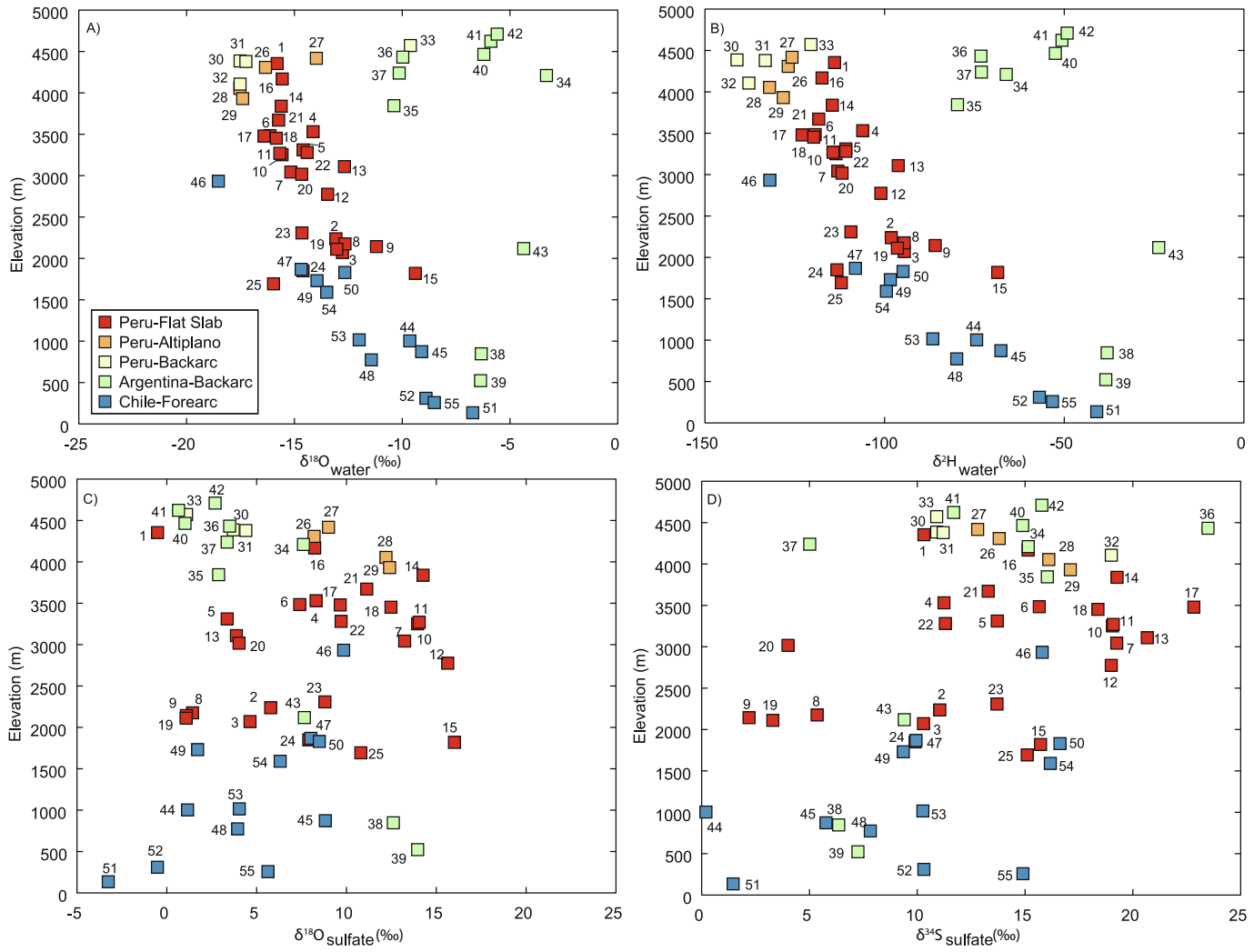

Fig. 6. Vector art file containing 4 plots of isotope ratios vs spring sample elevation.
(A-B) Changes of δ2H and δ18O of thermal water and (C—D) δ18O and δ34S of dissolved sulfate relative to elevation. Numbers refer to locations of sampling points presented on Fig. 3.

microbial sulfate reduction are common in marine sediments (Canfield, 2001). In subduction zones, these S endmembers are proposed to be ejected from the subducted marine sediments as a result of compaction, heating and devolatilization (Tomkins and Evans, 2015). In the Central Andes, direct release of slab-derived SO_4^{2-} into deeply sourced thermal springs would result in high $\delta^{34}S$ and $\delta^{18}O$ values similar to the Pliocene-Miocene seawater (~ + 20 ‰ and + 12 ‰, respectively; Claypool et al., 1980) that was present in the marine sediments prior to subduction. Note that these values would be higher if microbial sulfate reduction were occurring prior to subduction because this process leads to significant increases of $\delta^{34}S$ and $\delta^{18}O$ in the pore-water SO_4^{2-} (Canfield, 2001). On the other hand, any measurable input of SO_4^{2-} from devolatilization and oxidation of biogenic H_2S/sulfide minerals would significantly decrease its $\delta^{34}S$ (Krouse and Mayer, 2000). Generally, variable inputs of pore-water- and sulfide-derived SO_4^{2-} would result in a wide range of $\delta^{34}S$, from −45 ‰ to +14 ‰ (see summary Suppl. Table 2). In contrast, any significant inputs of S/SO_4^{2-} from the mantle into the thermal springs would lead to narrow ranges of $\delta^{34}S$, −1.5 ‰ to 0 ‰ (Sakai et al., 1984; Labidi et al., 2013). While mixing processes may lead to wider ranges of $\delta^{34}S$, it is expected that the $\delta^{18}O$ of slab-derived SO_4^{2-} would be distinctive with higher values than in the initial marine SO_4^{2-} (+12 ‰). This is because of expected oxygen isotope exchange between SO_4^{2-} and the pore-water/fluids usually with higher $\delta^{18}O$ values (Sheppard, 1986). While this exchange is relatively slow under surface temperature conditions (~10^5 to 10^6 years; Lloyd, 1968), the prolonged duration (millions of years) of subduction processes would likely lead to measurable increases of $\delta^{18}O$ of SO_4^{2-} under higher (subsurface) temperatures. For instance, under temperatures found at the slab interface (450–900 °C) the oxygen isotope exchange would lead to increases of $\delta^{18}O$ in SO_4^{2-} by 0.5 to 3 ‰ compared to the fluid, and by 5 to 20 ‰ under geothermal conditions (100–300 °C) (Lloyd, 1968; Mizutani and Rafter, 1969; Mizutani, 1972). Therefore, it can be expected that the $\delta^{18}O$ of SO_4^{2-} could reach values as high as +30 ‰ in the presence of subduction fluids that underwent substantial oxygen isotope exchange with SO_4^{2-}.

Thermal springs controlled by groundwater flow paths along active and large-displacement normal faults in the studied areas (Fig. 1b–e) have the greatest potential for recording inputs of slab-derived SO_4^{2-} and H_2S volatilization due to the presence of other mantle-derived volatiles in these setting (Newell et al., 2015; Scott et al., 2020). Because of their higher permeability, these features act as potential conduits between deeply derived fluids/gases and shallow meteoric water (Dipple and Ferry, 1992; Baumgartner and Valley, 2001). Therefore, they are expected to experience the largest contribution of deeply sourced SO_4^{2-} and water with distinctive (higher) $\delta^{18}O$ values due to oxygen isotope exchange. This is of particular interest for the thermal springs above the flat slab, where temperature conditions affecting the oceanic slab are lower than in the steeply dipping subduction zones (Manea and Manea,

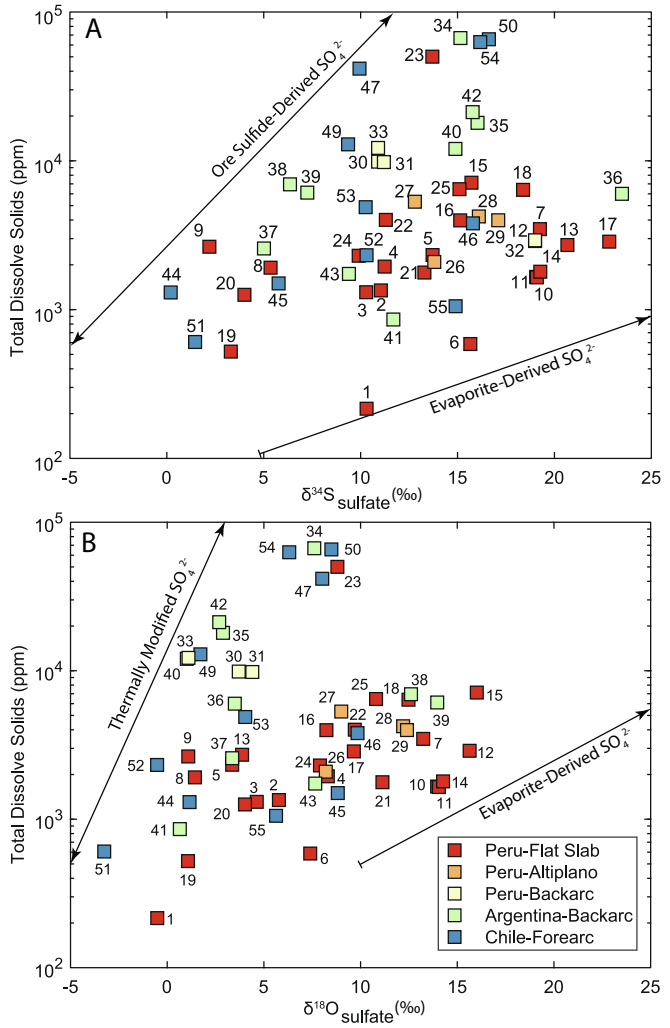

Fig. 7. Vector art file containing two plots of stable isotope ratios in sulfate vs total dissolved solids.
(A) $\delta^{34}S$ and (B) $\delta^{18}O$ of dissolved sulfate vs. total dissolved solids (TDS) in the Andean thermal springs. Numbers refer to locations presented in Fig. 3. Arrows indicate possible mixing trends between sulfide- and evaporite-derived sulfate sources based on previously reported bedrock isotope compositions (See Table S2 for compiled references with individual bedrock descriptions).

2011). Transfer of deeply sourced S is also likely adjacent to the slab transition area of the Altiplano Plateau and Chilean Central Valley Fault Zone (CVFZ) based on similar detection of deep volatiles (e.g., Ray et al., 2009; Hiett et al., 2021). However, there is no notable difference in the isotope composition of SO_4^{2-} and water between fault-controlled thermal springs (e.g., Locations 5–7, 28, 35–36, 38, 39, 43, 44–45, 52, & 54) and non-fault-controlled springs (Locations 8–10, 13–21, 29–33, 37, 40–42, 53, 55). They all showed similar ranges of $\delta^{34}S$ and $\delta^{18}O$ values in dissolved SO_4^{2-} (0 to +23 ‰ and − 3 to +16 ‰, respectively) and negative $\delta^{18}O$ of the spring water (−19 to −3 ‰). Also, there were no important differences in isotope composition of SO_4^{2-} between thermal springs in steep- and flat-subduction settings (Figs. 2, 4). Furthermore, the fault-controlled springs did not show evidence of H_2S degassing (e.g., no rotten egg odor) at the time of sampling. This suggests that most thrust faults in the Andes do not appear to act as direct conduits for S transfer from deep crustal sources to the near surface. Instead, shallow sources of S are more apparent (see Section 5.2. for details).

This conclusion is further supported by distinctive negative $\delta^{18}O$ and $\delta^{2}H$ values of all thermal spring water that closely mirror the global meteoric water line (GMWL), suggesting groundwater sourced by meteoric precipitation in the studied subduction settings (Craig, 1961), as is expected and observed for continental hot springs globally. This contradicts the potential for detectable aqueous transport of slab or mantle-derived S/SO_4^{2-} inputs to the upper crustal rocks. Only springs associated with lower discharges and higher temperatures (60–84 °C) deviate to the right of the GMWL (Fig. 5). This variance is consistent with rock-water isotope exchange at elevated temperature, leading to increases of $\delta^{18}O$ (Gat, 1996). Additionally, there is a strong negative correlation between $\delta^{18}O$ and $\delta^{2}H$ values of the thermal springs and elevation across all locations (Fig. 6b–c). This trend follows an altitude effect observed for the Andean precipitation across the region (Rozanski and Araguas Araguas, 1995; Poage and Chamberlain, 2001; Newell et al., 2015; Bershaw et al., 2016; Scott et al., 2020), thus further supports local water sourcing for the studied thermal springs, mainly from shallow meteoric circulation.

Furthermore, the difference between the $\delta^{18}O$ of SO_4^{2-} and $\delta^{18}O$ of thermal spring water (expressed as $\Delta^{18}O_{SO4\text{-}H2O}$) is useful in assessing whether the dissolved SO_4^{2-} is associated with groundwater flow paths exposed to higher temperatures at depth. Under low temperature conditions (<50 °C) and short timescales (years to thousands of years), oxygen isotope exchange between SO_4^{2-} and water is negligible (Lloyd, 1968). However, the SO_4^{2-} in groundwater associated with higher temperatures (>100 °C) would show distinctive $\Delta^{18}O_{SO4\text{-}H2O}$ because of rapid (days to years) oxygen isotope exchange between SO_4^{2-} and water (Lloyd, 1968; Van Stempvoort and Krouse, 1993). Many of the studied thermal springs showed elevated temperatures (>50–84 °C) at the time of sampling (Fig. 8). However, at depth and near active volcanic centers the temperatures of geothermal fluids could reach 200–300 °C, as previously observed in subsurface geothermal reservoirs associated with active volcanism (Goff et al., 1988). According to Lloyd (1968), the $\Delta^{18}O_{SO4\text{-}H2O}$ is ~20 ‰ at 84 °C and ~ 5 to 9 ‰ at 200–300 °C (Fig. 8). In contrast, the studied thermal springs showed a wider range of $\Delta^{18}O_{SO4\text{-}H2O}$, from 3 to 30 ‰ (Fig. 8). While three thermal springs near active volcanic centers (Locations 40–42) showed lower $\Delta^{18}O_{SO4\text{-}H2O}$ values (6–8 ‰) consistent with oxygen isotope exchange at higher temperatures of 200–300 °C at depth; this was not the case in Location 46 with higher $\Delta^{18}O_{SO4\text{-}H2O}$. However, unlike Locations 40–42 the spring at Location 46 discharges from marine sedimentary formations rather than volcanic flows, thus any SO_4^{2-} input from dissolution of evaporites with higher $\delta^{18}O$ would result in higher $\Delta^{18}O_{SO4\text{-}H2O}$. The overall wide range of $\Delta^{18}O_{SO4\text{-}H2O}$ suggests limited exposure to higher temperatures in which the oxygen isotope exchange would occur relatively fast (Lloyd, 1968). This, in turn, implies relatively short residence time of SO_4^{2-} in the studied thermal springs, which is consistent with similar findings based on carbon and nitrogen isotopes in the Peruvian thermal springs (Hiett et al., 2022). Alternatively, the highest $\Delta^{18}O_{SO4\text{-}H2O}$ values of the studied thermal springs might be recording complete oxygen isotope exchange at elevated temperatures with depth prior to fluid ascent. However, the $\delta^{18}O$ of ascending thermal water would not show a strong relationship with elevation as is evident in many of the studied thermal springs (Fig. 6a). Generally, the altitude-controlled $\delta^{18}O$ signature accompanies shallow circulation of meteoric fluids and diminishes with increasing groundwater flow paths, circulation depths, and elevated temperature. This is mainly due to mixing processes associated with meteoric water recharge at different elevations and increasing water-rock interaction along groundwater flow path (e.g., Gat, 1996; Krouse and Grinenko, 1992).

In summary, our isotope results suggest negligeable, if any, contributions of slab-derived S/SO_4^{2-} and deep fluids into the Andean thermal springs. This might be because slab temperatures in non-magmatic and flat slab settings are too low to drive devolatilization and thermal release of S from the oceanic slab. Also, the S could be rapidly sequestered near the point of release due to precipitation of S minerals within the bedrock as proposed for deep-slab settings (Walters et al., 2019) and/or during later water-rock interactions in the lower/upper crust (Henley and Fischer, 2021; de Moor et al., 2022). This, in turn, is consistent with the increased abundances of sulfide minerals found in the exhumed rocks of

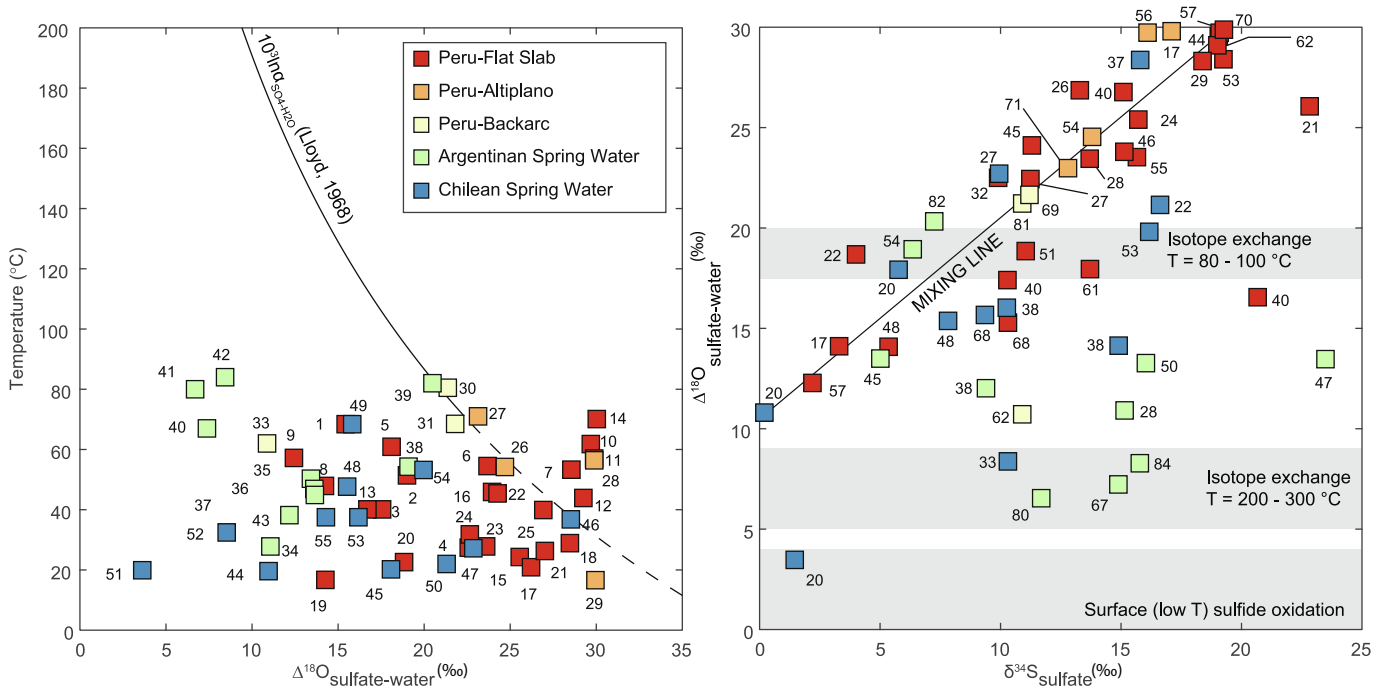

Fig. 8. Vector art file containing two plots. One of $\Delta^{18}O_{SO4\text{-}H2O}$ against spring discharge temperature and one of sulfate $\delta^{34}S$ vs $\Delta^{18}O_{SO4\text{-}H2O}$.
(A) Changes of $\Delta^{18}O_{SO4\text{-}H2O}$ relative to the temperature of thermal springs measured at the time of sampling. Solid and dashed lines indicate temperature-dependent oxygen isotope fractionation between sulfate and water determined via experiments for high temperatures and theoretical estimation for low temperatures, respectively (after Lloyd, 1968). Numbers next to the symbols refer to the locations of sampling points presented on Fig. 3. (B) Changes of $\delta^{34}S$ of sulfate relative to $\Delta^{18}O_{SO4\text{-}H2O}$. The black line indicates a possible mixing between evaporite- and sulfide-derived sulfate (black line) in shallow low temperature environment. Grey boxes correspond to the predicted $\Delta^{18}O_{SO4\text{-}H2O}$ values for complete oxygen isotope exchange at higher temperatures of 80–100 °C and 200–300 °C in comparison to the low temperature sulfide oxidation in surface settings. Numbers next to the symbols refer to the measured temperatures of thermal springs.

lower crustal and mantle wedge from past orogenic activities, thus we infer this might also be the case in the flat slab settings (Tomkins and Evans, 2015; Lee et al., 2018; Rielli et al., 2018; Walters et al., 2019). Additionally, it is likely that greater contributions of crustal/shallow S (e.g., dissolution of marine evaporites, oxidation of ore deposits), as well as secondary reactions in the shallow subsurface (e.g., Henley and Fischer, 2021) may mask minor S inputs from the subducted slab due to the limited transport pathways for deeply derived S to influence thermal fluids in the upper crustal reservoirs.

5.2. Assessment of shallow SO_4^{2-} sources in thermal springs

In the absence of direct contributions of slab-derived S, it is important to determine if the elevated SO_4^{2-} concentrations of the Andean thermal springs result from water-rock interaction in the upper crust and/or chemical weathering in surface environments. S and O isotope tracers are useful in determining shallow SO_4^{2-} sources and groundwater flow paths because of wide variation of $\delta^{34}S$ and $\delta^{18}O$ in the lithosphere and hydrosphere (e.g., Clark and Fritz, 1997). Sulfur isotope fractionations during oxidation/dissolution of S-bearing minerals such as sulfates and sulfides are minor/negligible, thus the $\delta^{34}S$ of SO_4^{2-} in surface water and shallow groundwater preserves the initial composition of the bedrock (e.g., Krouse and Grinenko, 1992). During dissolution of sulfate minerals, O isotope fractionations are negligible and aqueous SO_4^{2-} preserves the high/positive $\delta^{18}O$ values of marine evaporites. In contrast, during oxidation of sulfide minerals, the O isotope composition of sulfide-derived SO_4^{2-} usually preserves low/negative $\delta^{18}O$ of meteoric water with minor enrichment in heavier ^{18}O isotopes. (e.g., (Krouse and Grinenko, 1992).

In the studied areas of central Andes (Figs. 1, 3), the lithologic S-rich sources exposed at the surface or identified in the shallow subsurface are: 1) Jurassic to Paleogene sulfate and biogenic sulfide minerals in marine evaporites and sediments (Coney, 1964; Horton et al., 2001, 2016; DeCelles et al., 2011; Carrapa et al., 2012; Scherrenberg et al., 2012; Horton, 2018a; Sundell et al., 2018), 2) Cretaceous to Neogene S-bearing ore deposits (Petersen, 1965; Fontboté et al., 1990; Scherrenberg et al., 2016), and 3) Cretaceous to modern igneous rocks and S devolatilization of active magma bodies (Coney, 1971; Cobbing, 1982; Coira et al., 1982; Jordan et al., 1983; Parada et al., 1988; Garver et al., 2005; Maloney et al., 2013). The sulfides of magmatic origin show lower $\delta^{34}S$ values with narrower ranges (0 to +11 ‰) compared to higher values and wider ranges in the sulfide-rich ores (0 to +18 ‰) (Fig. 9). While the $\delta^{34}S$ of marine evaporites widely varies (+14 to +32 ‰ in Peru, +5 to +42 ‰ in Argentina, +7 to +42 ‰ in Chile), their $\delta^{18}O$ values are distinctively high and vary in a smaller range (+10 to +20 ‰) (Fig. 9, see Suppl. Table 3 for references).

Fig. 9 illustrates a positive relationship between $\delta^{34}S$ and $\delta^{18}O$ values of SO_4^{2-} measured in the studied thermal springs that are generally consistent with spatial distribution and isotope composition of bedrock sulfate and sulfide minerals across the studied region (Fig. 3). This implies significant mixing of SO_4^{2-} from dissolution of marine evaporites and oxidation of diagenetic/magmatic ore sulfide minerals present in the local bedrock. The spatial relationships also inform potential flow paths of the studied thermal water beneath these flows. For example, in the Argentinean backarc the thermal springs flowing out of volcanic units (~200–400 m thick; Coutand et al., 2001) often have higher $\delta^{34}S$ and $\delta^{18}O$ values (Locations 34–36) that are more consistent with marine evaporites in the underlying sedimentary strata rather than magmatic sulfides present in the overlying volcanic units. This would suggest rather shallow water circulation that penetrates beneath surficial volcanic deposits but does not interact with magmatic S degassing and plumbing systems at depth. Alternatively, the higher $\delta^{34}S$ and $\delta^{18}O$ of SO_4^{2-} might also be controlled to some degree by atmospheric deposition of sea aerosols that are common along the Central Andes (e.g., Arenas-Díaz et al., 2022). The sea spray has similar isotope composition of SO_4^{2-} as the bedrock evaporites, thus the surface leaching by meteoric

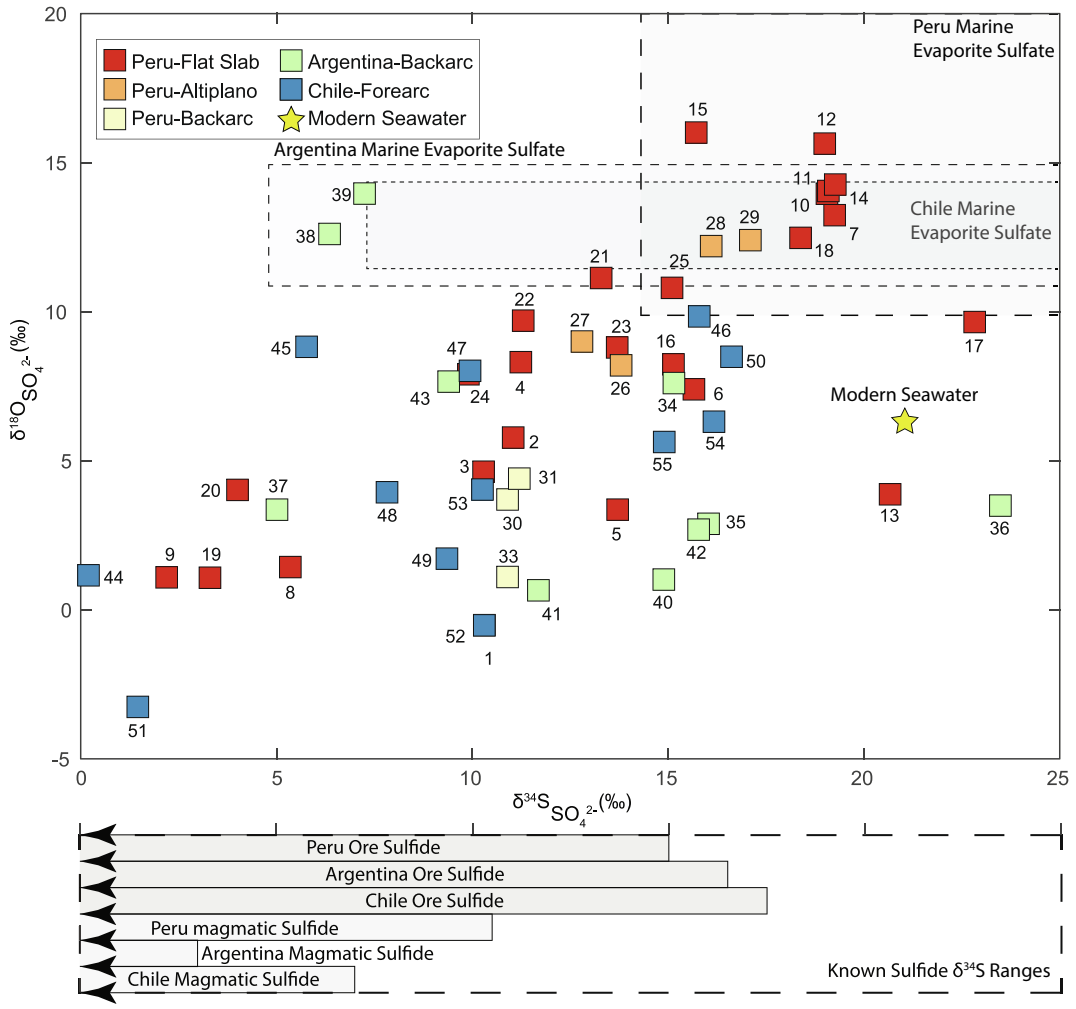

Fig. 9. Vector art file containing plot of measured spring sulfate $\delta^{34}S$ vs $\delta^{18}O$ and ranges of bedrock sulfate $\delta^{34}S$ vs $\delta^{18}O$ and sulfur sulfate $\delta^{34}S$. Variation of $\delta^{34}S$ and $\delta^{18}O$ in the dissolved sulfate from the Andean thermal springs. Shaded and dashed boxes are the known ranges of isotope composition for local marine evaporites. Brown and light grey bars below x-axis show the ranges of $\delta^{34}S$ values in local magmatic- and ore-derived sulfide minerals, respectively. Black arrows within sulfide ranges indicate the $\delta^{34}S$ values below 0 ‰ in some sulfide phases of the study areas. Numbers refer to the locations of sampling points presented in Fig. 3. (For interpretation of the references to colour in this figure legend, the reader is referred to the web version of this article.)

precipitation would be increasing the $\delta^{34}S$ and $\delta^{18}O$ of SO_4^{2-} in the groundwater systems of the studied areas.

While minor contribution of magmatic S/SO_4^{2-} to the thermal springs cannot be ruled out entirely in volcanically active regions, there is little support for this process in the studied Andean settings. For example, at Locations 46, 47, and 54 the thermal springs occur in closer proximity to active volcanic centers (< 25 km) but have similar $\delta^{34}S$ values (+9.9 to +16.2 ‰) to the local marine evaporites rather than in the modern volcanic pyrite/glasses (−0.6 to +7 ‰) of Argentina and Chile (Suppl. Table S2). In addition to the inputs of sea aerosols, the increasing $\delta^{34}S$ values of SO_4^{2-} at these volcanic locations could also be driven by sulfide precipitation in the shallow subsurface during hydrothermal S degassing (de Moor et al., 2022). On the other hand, in Locations 33–34 located within ~40 km from active volcanoes and within the zone of modern arc magmatism, the $\delta^{34}S$ and $\delta^{18}O$ values of SO_4^{2-} (+10.9 to +15.2 ‰ and + 1.1 to +7.6 ‰, respectively) also closely reflect the isotopic composition of the nearby ore deposits oxidized by meteoric waters ($\delta^{34}S = -5.9$ to +15 ‰; (Petersen, 1965; Ripley and Ohmoto, 1977; Campbell and Rye, 1982; Bartlett, 1984; Campbell, 1987; Fontboté and Gorzawski, 1990; Rye, 1993; Parnell et al., 1994; Polliand et al., 1999; Schutfort, 2001; Echavarria et al., 2006; Baumgartner et al., 2008; Suzuki and Hayashi, 2019; Voute et al., 2019). Generally, the lack of clear SO_4^{2-} inputs from direct devolatilization of magmatic S (e.g., H_2S or SO_2 gas with lower/ magmatic $\delta^{34}S$ values) into the thermal springs suggest considerable S suppression in a deeper subduction environment before any interaction with shallow groundwater occurs (see Section 5.1 for more details).

The $\delta^{34}S$ values of bedrock sulfide minerals show large variations across the studied regions of the central Andes, often overlapping with $\delta^{34}S$ values of marine evaporites (Fig. 9). This is particularly true for ore sulfide minerals with higher $\delta^{34}S$ values (+10 to +18 ‰) derived from assimilation of sedimentary S during past hydrothermal activity (Gorzawski et al., 1990; Gemmell et al., 1992; Carrillo-Rosúa et al., 2014). However, these two sources of SO_4^{2-} can be distinguished based on $\delta^{18}O$ values. For example, the $\delta^{18}O$ values of SO_4^{2-} in marine evaporites is high and varies in a narrow range (+10 to +20 ‰; Fig. 9) compared to the expected lower $\delta^{18}O$ values of sulfide-derived SO_4^{2-}. This is because during oxidation of ore sulfide minerals the SO_4^{2-} incorporates oxygen from meteoric water with lower (negative) $\delta^{18}O$ values (Van Stempvoort and Krouse, 1993; Krouse and Mayer, 2000) controlled in part by the $\delta^{18}O$ of local precipitation (<−3 ‰; Fig. 6c). Despite higher $\delta^{34}S$ values, a significant number (16) of the studied thermal spring showed distinctive lower $\delta^{18}O$ values of SO_4^{2-} (<+10 ‰) consistent with the inputs from oxidation of sulfide with higher $\delta^{34}S$ values (Fig. 9). As a result, the $\delta^{18}O$ of spring SO_4^{2-} often falls off a simple mixing line between the ^{18}O-enriched SO_4^{2-} from marine evaporite minerals and ^{18}O-depleted sulfide-derived SO_4^{2-} (Fig. 9). Additionally,

the measured $\delta^{34}S$ and $\delta^{18}O$ of sulfide- and evaporite-derived SO_4^{2-} in the studied springs can be spatially correlated with known distribution of porphyry ore deposits and marine evaporites in central Andes (Figs. 1, 3). This indicates that the SO_4^{2-} is sourced from the near-surface deposits. While a clear distinction between various sulfide-derived SO_4^{2-} sources (magmatic- and ore-derived) is not always possible in the studied areas, their mixing with the marine evaporite end members (and to some degree sea aerosols) clearly controls the isotopic composition of SO_4^{2-} in the Andean thermal springs. The latter is also supported by a lack of correlation between the $\delta^{18}O$ of sulfate and altitude, high $\Delta^{18}O_{SO4\text{-}H2O}$ values, and overall higher $\delta^{18}O$ of SO_4^{2-} (Figs. 6c-d, 8a). If only sulfide-derived SO_4^{2-} comprised the thermal spring water, low $\Delta^{18}O_{SO4\text{-}H2O}$ values and similar negative correlation with altitude would be apparent in the $\delta^{18}O$ of SO_4^{2-}, as it is observed for the $\delta^{18}O$ of spring water and altitude (Fig. 6c).

In summary, there is little to no evidence for the $\delta^{34}S$ and $\delta^{18}O$ to be directly controlled by the slab-derived S/SO_4^{2-} (see Section 5.1 for details). Conversely, the systematic relationship of isotope compositions of SO_4^{2-} with known upper crustal lithologies (marine evaporites, ore sulfides, etc.) accompanied by negative $\delta^{18}O$ of meteorically derived spring water points to the main SO_4^{2-} inputs from near surface environments along shallow groundwater flow paths. The prevalence of higher $\delta^{34}S$ and $\delta^{18}O$ consistent with sediment-bound marine evaporites and atmospheric deposition of sea aerosols solidifies this relationship and supports upper-crustal SO_4^{2-} sourcing for the Andean thermal springs.

5.3. Sulfur cycle in the cordilleran subduction settings

Our new isotopic results suggest that the dissolved SO_4^{2-} in thermal springs of the long-lived Cordilleran margins such as the Andes does not originate from direct (modern) S inputs from the subducted oceanic slab or adjacent magmatic emissions. Instead, the SO_4^{2-} contributions are controlled by dissolution and oxidation of bedrock S-bearing minerals formed during complex orogenic history of the region. This is evident from the wide ranges of $\delta^{34}S$ and $\delta^{18}O$ values of dissolved SO_4^{2-} that closely reflect isotope composition of local bedrock comprised of S-bearing ores as well as igneous and sedimentary rocks. In each of the studied tectonomagmatic settings, distinctive $\delta^{34}S$ and $\delta^{18}O$ of bedrock minerals are the result of multiple processes related to orogenic history of the Andes (Fig. 10). For example, the $\delta^{34}S$ and $\delta^{18}O$ of dissolved SO_4^{2-} in thermal springs located in areas with recent surface uplift and thick sedimentary successions (e.g., Peruvian flat slab and slab transition, Peruvian and Argentine backarcs) resemble the composition of Jurassic - Cretaceous evaporites and subsequently formed S-rich ore mineralization. Whereas in the regions with extensive young volcanic flows or shallow/exposed plutons (e.g., Chilean forearc), the $\delta^{34}S$ values of SO_4^{2-} are consistent with oxidation of igneous sulfides.

The close relationship between distinctive higher $\delta^{34}S$ and lower $\delta^{18}O$ values, elevated SO_4^{2-} concentrations, decreasing pH of spring water, and spatial distribution of the mined ore S deposits (Figs. 1, 9, 10) highlights the importance of sulfide oxidation in the S/SO_4^{2-} budget of the studied thermal springs. This is because Paleogene-modern ore sulfide minerals coupled with oxidation of S in organic-rich shales are the most abundant S source in the Andean lithologic units. In comparison, Jurassic-Cretaceous marine evaporites bound in sedimentary units are a profoundly less volumetrically significant S source for these fluids. Even lower S abundances in the Cretaceous to modern volcanic and plutonic rocks indicates that sulfide oxidation from within these lithologies is detectable only when they are the sole source of S available to spring water. This may also explain the lack of a detectable signature for the

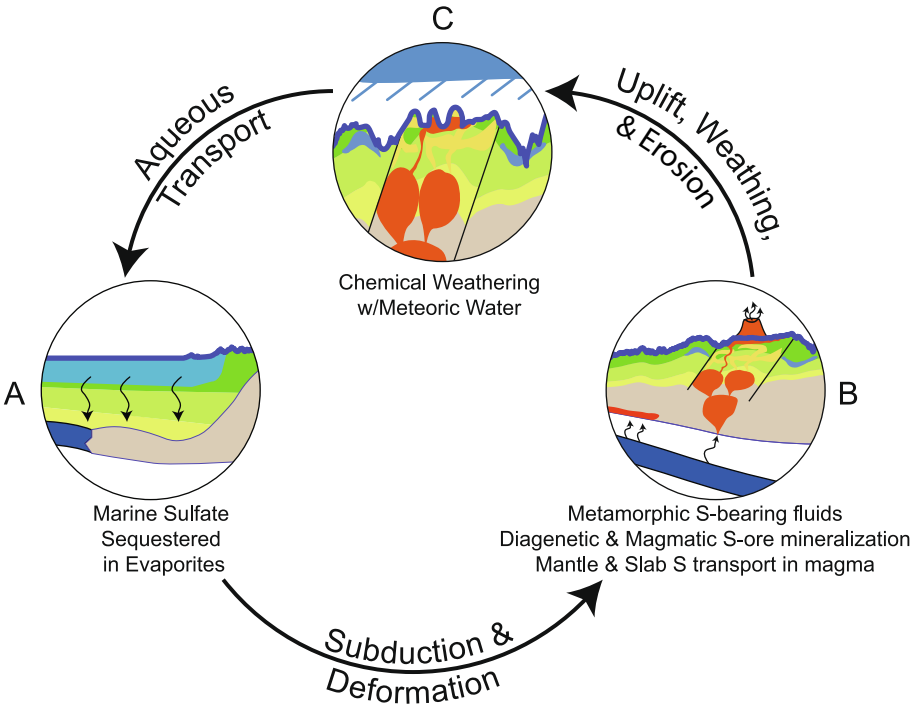

Fig. 10. Vector art file containing a schematic cartoon of the orogenic sulfur cycle based on tectonic history of Andes and spring sulfate isotope composition. Conceptual model of S cycle recorded in the isotope composition of dissolved sulfate in the modern Andean thermal springs. (A) Initially, S is trapped in marine sediment as porewater sulfate, biogenic sulfide, and evaporite minerals. (B) Following initiation of subduction, these marine sediments are uplifted and deformed, leading to formation of the supracrustal sequences found throughout the central Andes. Concurrently, subduction-related melting occurs leading to some S sequestration in plutonic rocks and magmatic sulfide-rich ore deposits. Additional sediment-bound S becomes concentrated and incorporated into diagenetic sulfide ore deposits formed during tectonic deformation. (C) As subduction-related exhumation continues, bedrock sulfate and sulfide minerals are brought to the near surface, where they intersect groundwater flow paths. This leads to dissolution of marine evaporite-derived sulfate and oxidation of ore and magmatic sulfide minerals, which contribute the dissolved sulfate to the thermal spring water. The spring water mixes with surface water in creeks and rivers that transport the dissolved sulfate back to the global ocean.

modern slab-derived S in the studied thermal springs regardless of the subduction angle and/or proximity to the trench. Previous studies have shown that in steeply dipping subduction zones, S liberated from the subducting slab reacts readily with O and iron (Fe) in the mantle wedge and the lower to middle crust, leading to S sequestration during formation of metamorphic sulfide assemblages in the lower crust and S-bearing ore minerals at higher crustal positions (Lee et al., 2018; Walters et al., 2019, 2020). It is possible that similar processes occur in the Andean flat slab settings under lower pressure-temperature conditions. Alternatively, lower fracture density and relative permeability at depths and along deep fault networks may limit degassing and aqueous solute transport, including H_2S and dissolved SO_4^{2-}, from the slab interface to the upper and middle crust by occluding material flow within timescales relevant to this study.

We propose that the isotope composition of dissolved SO_4^{2-} in thermal springs across the studied Cordilleran orogenic settings is mainly controlled by liberation of S earlier sequestered throughout the entirety of the mountain building event (Fig. 10). The sequestration process began prior to initiation of subduction along western South America when marine S (e.g., evaporites, pore-water SO_4^{2-}, biogenic sulfides/H_2S) was deposited on the sea floor followed by burial and lithification. During subduction in the Cretaceous, these marine deposits were uplifted and deformed along with the continental margin. Compression and tectonic burial resulted in formation of metamorphic and diagenetic ores, with bedrock S assimilation forming sulfide ore deposits within the deforming marine sediments (Fontboté and Gorzawski, 1990). Meanwhile, subduction-related melting resulted in voluminous magmatic intrusion and volcanism (Maloney et al., 2013) and generated widespread sulfide ore deposits during magmatic-hydrothermal circulation (Deen et al., 1994) and residual sulfide minerals during crystallization of lavas and magmas (Rye, 2005; Arehart et al., 2013). These S-bearing deposits were then differentially uplifted due to the variations in subduction style along the Andean margin, where they are currently exposed to circulation of groundwater sourced by meteoric precipitation. The latter leads to subsequent dissolution of marine evaporites and oxidation of sulfide minerals. After discharge on the surface, the cycle continues as the thermal spring water undergoes mixing with surface water in creeks and rivers which transport the dissolved SO_4^{2-} back to the ocean.

6. Conclusion

The studied thermal springs from throughout the central Andes provide no direct evidence for the slab to surface transfer of S/SO_4^{2-} via groundwater circulation or along fault networks, regardless of subduction angle or the presence of active magmatism. Instead, the wide ranges of $\delta^{34}S$ and $\delta^{18}O$ values of dissolved SO_4^{2-} in thermal springs from across the Andes reflect the highly variable composition of S-bearing bedrock minerals present along groundwater flow paths in the upper crust. Liberation of this lithologically-bound S into thermal water represents late stages of water-rock interaction and chemical weathering in a complex orogenic S cycle. This cycle encompasses the entirety of the mountain building event including the deposition and crystallization of primary S minerals derived from seawater and passive margin sediments before the onset of subduction, later compression and uplift associated with subduction, as well as intrusion, eruption, and crystallization of magma, and migration of ore forming fluids. Consequently, the spatial distribution of these S-bearing lithologies is related to specific geodynamic conditions unique to each tectonomagmatic province across the South American margin.

The low δ^2H and $\delta^{18}O$ values of thermal springs are consistent with infiltration of locally derived meteoric water at these latitudes and altitudes. In particular, the lower $\delta^{18}O$ values of SO_4^{2-} are consistent with weathering of sulfide minerals in the presence of isotopically depleted meteoric water. Whereas $\delta^{34}S$ and $\delta^{18}O$ values of SO_4^{2-} cannot confirm deeper S inputs from modern subduction-related processes, the thermal springs prove to be a sensitive indicator of the upper crust and surface water-rock interactions at different temperatures in the Cordilleran margins.

Funding sources

This work was supported by the National Science Foundation [NSF-EAR-1623034, NSF-EAR-1623023] awarded to D. Newell and M. Jessup (Peru); the Sloan Foundation [grant number G-2016-7206] awarded to K. Lloyd, P. Barry, D. Giovannelli, and J.M. de Moor (Argentina); and an award from the Simons Foundation to K. Lloyd (Chile) [grant number 404586]. D.G. was also supported by funding from the European Research Council (ERC) under the European Union's Horizon 2020 research and innovation program Grant Agreement No. 948972-COEVOLVE-ERC-2020-STG. Additional support came from The National Fund for Scientific and Technological Development of Chile (FONDECYT) Grant 11191138 (The National Research and Development Agency of Chile, ANID Chile) and COPAS COASTAL ANID FB210021 to GJ.

CRediT authorship contribution statement

Tyler A. Grambling: Writing – original draft, Visualization, Methodology, Investigation, Formal analysis, Data curation. **Dennis L. Newell:** Writing – review & editing, Supervision, Resources, Project administration, Investigation, Funding acquisition, Formal analysis. **Karen G. Lloyd:** Writing – review & editing, Resources, Project administration, Investigation, Funding acquisition, Formal analysis, Data curation, Conceptualization. **Coleman D. Hiett:** Writing – review & editing, Resources, Investigation, Formal analysis, Data curation. **Heather Upin:** Writing – review & editing, Investigation. **Peter H. Barry:** Writing – review & editing, Investigation, Funding acquisition. **Donato Giovannelli:** Writing – review & editing, Investigation, Funding acquisition. **J. Maarten de Moor:** Writing – review & editing, Investigation, Funding acquisition. **Agostina Chiodi:** Writing – review & editing, Investigation, Funding acquisition. **Gerdhard L. Jessen:** Writing – review & editing, Investigation, Funding acquisition. **Jenny M. Blamey:** Writing – review & editing, Investigation. **Anna Szynkiewicz:** Writing – original draft, Visualization, Validation, Supervision, Resources, Project administration, Methodology, Investigation, Formal analysis, Conceptualization.

Declaration of competing interest

The authors declare that they have no known competing financial interests or personal relationships that could have appeared to influence the work reported in this paper.

Data availability

Geochemical and isotopic data used to support the findings of this study is available in the EarthChem (http://earthchem.org/) online data repository: Grambling, T. A., Newell, D. L., Lloyd, K. G., Hiett, C. D., Upin, H., Barry, P. H., Giovannelli, D., de Moor, J., Chiodi, A., Jessen, G. L., Blamey, J., Szynkiewicz, A., 2024. Isotopic ratios of sulfur and oxygen from sulfate in Andean thermal springs, Version 1.0. Interdisciplinary Earth Data Alliance (IEDA). https://doi.org/10.60520/IEDA/113086. Embargoed until Dec. 1st, 2024.

Acknowledgements

We thank A. Cafferata for field support and logistics in Peru, and endorsements from Dr. Jose Cardenas and the Universidad Nacional de San Antonio Abad de Cusco for our field expeditions in Peru. We also thank Anthony Faiia, Rhianna Moore, and Jessica Ende of the University of Tennessee Stable Isotope Laboratory for assistance with sample preparation and analysis. Comments from Simon Bottrell and an

anonymous reviewer are greatly appreciated.

Appendix A. Supplementary data

Supplementary data to this article is included as an excel spreadsheet containing three tables: Supplementary Table 1 with sample locations, measured isotopic ratios, and geochemical parameters; Supplementary Table 2 with the reported $\delta^{34}S$ values of sulfate and sulfide minerals from the studied areas published by different research groups; Supplementary Table 3, which contains full citations for isotope ratios in Suppl. Table 2. Supplementary data to this article can be found online at https://doi.org/10.1016/j.chemgeo.2024.122365.

References

Alt, J.C., Garrido, C.J., Shanks, W.C., Turchyn, A., Padrón-Navarta, J.A., López Sánchez-Vizcaíno, V., Gómez Pugnaire, M.T., Marchesi, C., 2012. Recycling of water, carbon, and sulfur during subduction of serpentinites: a stable isotope study of Cerro del Almirez, Spain. Earth Planet. Sci. Lett. 327–328, 50–60. https://doi.org/10.1016/j.epsl.2012.01.029.

Arehart, G.B., DeYoung, S., Poulson, S.R., Heaton, J.S., Weiss, S., 2013. Sulfur isotopes in plutonic rocks of the great basin as indicators of crustal architecture. J. Geol. 121, 355–369. https://doi.org/10.1086/670651.

Arenas-Díaz, F., Fuentes, B., Reyers, M., Fiedler, S., Böhm, C., Campos, E., Shao, Y., Bol, R., 2022. Dust and aerosols in the Atacama Desert. Earth Sci. Rev. 226, 103925 https://doi.org/10.1016/j.earscirev.2022.103925.

Armijo, R., Lacassin, R., Coudurier-Curveur, A., Carrizo, D., 2015. Coupled tectonic evolution of Andean orogeny and global climate. Earth Sci. Rev. 143, 1–35. https://doi.org/10.1016/j.earscirev.2015.01.005.

Atherton, M.P., Petford, N., 1996. Plutonism and the growth of Andean Crust at 9 °S from 100 to 3 Ma. J. S. Am. Earth Sci. 9, 1–9. https://doi.org/10.1016/0895-9811(96)00023-5.

Barry, P.H., et al., 2019. Forearc carbon sink reduces long-term volatile recycling into the mantle. Nature 568, 487–492. https://doi.org/10.1038/s41586-019-1131-5.

Barry, P.H., De Moor, J.M., Chiodi, A., Aguilera, F., Hudak, M.R., Bekaert, D.V., Giovannelli, D., 2022. The helium and carbon isotope characteristics of the Andean Convergent Margin. Front. Earth Sci. 10, 897267. https://doi.org/10.3389/feart.2022.897267.

Bartlett, M.W., 1984. Petrology and Genesis of Carbonate-Hosted Pb-Zn-Ag Ores. Oregon State University, San Cristobal district, Department of Junin, Peru, 287 p.

Basuki, N.I., Taylor, B.E., Spooner, E.T.C., 2008. Sulfur isotope evidence for thermochemical reduction of dissolved sulfate in Mississippi Valley-type zinc-lead mineralization, Bongara area, Northern Peru. Econ. Geol. 103, 783–799. https://doi.org/10.2113/gsecongeo.103.4.783.

Baumgartner, L.P., Valley, J.W., 2001. Stable Isotope Transport and Contact Metamorphic Fluid Flow. Rev. Mineral. Geochem. 43, 415–467. https://doi.org/10.2138/gsrmg.43.1.415.

Baumgartner, R., Fontboté, L., Vennemann, T., 2008. Mineral zoning and geochemistry of epithermal polymetallic Zn-Pb-Ag-Cu-Bi mineralization at Cerro de Pasco, Peru. Econ. Geol. 103, 493–537. https://doi.org/10.2113/gsecongeo.103.3.493.

Bershaw, J., Saylor, J.E., Garzione, C.N., Leier, A., Sundell, K.E., 2016. Stable isotope variations (δ18O and δD) in modern waters across the Andean Plateau. Geochim. Cosmochim. Acta 194, 310–324. https://doi.org/10.1016/j.gca.2016.08.011.

Bloch, W., John, T., Kummerow, J., Salazar, P., Krüger, O.S., Shapiro, S.A., 2018. Watching Dehydration: Seismic Indication for Transient Fluid Pathways in the Oceanic Mantle of the Subducting Nazca Slab. Geochem. Geophys. Geosyst. 19, 3189–3207. https://doi.org/10.1029/2018GC007703.

Campbell, A.R., 1987. A Sulfur Isotopic Study of the San Cristobal Tungsten-Base Metal Mine, vol. 22. Mineralium Deposita, Peru, pp. 42–46. https://doi.org/10.1007/BF00204242.

Campbell, A.R., Rye, D.M., 1982. Fluid inclusion and stable Isotope study of the San Cristobal Mine, Peru. In: Geological Society of America Abstracts with Programs Vol. 14.

Canfield, D.E., 2001. Isotope fractionation by natural populations of sulfate-reducing bacteria. Geochim. Cosmochim. Acta 65, 1117–1124. https://doi.org/10.1016/S0016-7037(00)00584-6.

Carrapa, B., Bywater-Reyes, S., Decelles, P.G., Mortimer, E., Gehrels, G.E., 2012. Late Eocene-Pliocene basin evolution in the Eastern Cordillera of northwestern Argentina (25°-26°S): regional implications for Andean orogenic wedge development. Basin Res. 24, 249–268. https://doi.org/10.1111/j.1365-2117.2011.00519.x.

Carrillo-Rosúa, J., Boyce, A.J., Morales-Ruano, S., Morata, D., Roberts, S., Munizaga, F., Moreno-Rodríguez, V., 2014. Extremely negative and inhomogeneous sulfur isotope signatures in cretaceous Chilean manto-type Cu-(Ag) deposits, Coastal Range of central Chile. Ore Geol. Rev. 56, 13–24. https://doi.org/10.1016/j.oregeorev.2013.06.013.

Catchpole, H., Kouzmanov, K., Putlitz, B., Seo, J.H., Fontboté, L., 2015. Zoned base metal mineralization in a porphyry system: origin and evolution of mineralizing fluids in the Morococha District, Peru. Econ. Geol. 110, 39–71. https://doi.org/10.2113/econgeo.110.1.39.

Chiodi, A., Tassi, F., Báez, W., Maffucci, R., Invernizzi, C., Giordano, G., Pierantoni, P.P., 2015. New geochemical and isotopic insights to evaluate the geothermal resource of the hydrothermal system of Rosario de la Frontera (Salta, northern Argentina). J. Volcanol. Geotherm. Res. 295, 16–25. https://doi.org/10.1016/j.jvolgeores.2015.03.001.

Clark, I.D., Fritz, P., 1997. Environmental Isotopes in Hydrogeology. CRC Publishing, Boca Raton, 328 p.

Claypool, G.E., Holser, W.T., Kaplan, I.R., Sakai, H., Zak, I., 1980. The age curves of sulfur and oxygen isotopes in marine sulfate and their mutual interpretation. Chem. Geol. 28, 199–260. https://doi.org/10.1016/0009-2541(80)90047-9.

Cobbing, E.J., 1982. The segmented Coastal Batholith of Peru: its relationship to volcanicity and metallogenesis. Earth Sci. Rev. 18, 241–251. https://doi.org/10.1016/0012-8252(82)90039-3.

Cohen, A., McGlue, M.M., Ellis, G.S., Zani, H., Swarzenski, P.W., Assine, M.L., Silva, A., 2015. Lake formation, characteristics, and evolution in retroarc deposystems: a synthesis of the modern Andean orogen and its associated basins. In: Geodynamics of a Cordilleran Orogenic System: The Central Andes of Argentina and Northern Chile. Geological Society of America, pp. 309–335. https://doi.org/10.1130/2015.1212(16.

Coira, B., Davidson, J., Mpodozis, C., Ramos, V., 1982. Tectonic and magmatic evolution of the Andes of northern Argentina and Chile. Earth Sci. Rev. 18, 303–332. https://doi.org/10.1016/0012-8252(82)90042-3.

Coney, P.J., 1964. Geology and Geography of the Cordillera Huayhuas. University of New Mexico, Peru, 304 p.

Coney, P.J., 1971. Structural evolution of the Cordillera Huayhuash, Andes of Peru. Bull. Geol. Soc. Am. 82, 1863–1884. https://doi.org/10.1130/0016-7606(1971)82[1863:SEOTCH]2.0.CO;2.

Coutand, I., Cobbold, P.R., De Urreiztieta, M., Gautier, P., Chauvin, A., Gapais, D., Rossello, E.A., López-Gamundí, O., 2001. Style and history of Andean deformation, Puna plateau, northwestern Argentina. Tectonics 20, 210–234. https://doi.org/10.1029/2000TC900031.

Craig, H., 1961. Isotopic Variations in Meteoric Waters. Science 133, 1702–1703.

Daniele, L., Taucare, M., Roquer, T., Viguier, B., Sepúlveda, J., Molina, E., Morata, D., 2022. Fault-Related Thermal Springs: Water Origin and Hydrogeochemical Processes at Liquiñe Area (Southern Volcanic Zone, Chile). Authorea Preprints. https://doi.org/10.1002/essoar.10501117.2.

De Moor, J.M., Fischer, T.P., Plank, T., 2022. Constraints on the sulfur subduction cycle in Central America from sulfur isotope compositions of volcanic gases. Chem. Geol. 588, 120627 https://doi.org/10.1016/j.chemgeo.2021.120627.

Decelles, P.G., Ducea, M.N., Kapp, P., Zandt, G., 2009. Cyclicity in Cordilleran orogenic systems. Nat. Geosci. 2, 251–257. https://doi.org/10.1038/ngeo469.

DeCelles, P.G., Carrapa, B., Horton, B.K., Gehrels, G.E., 2011. Cenozoic foreland basin system in the Central Andes of northwestern Argentina: implications for Andean geodynamics and modes of deformation. Tectonics 30, 1–30. https://doi.org/10.1029/2011TC002948.

Deen, J.A., Rye, R.O., Munoz, J.L., Drexler, J.W., 1994. The magmatic hydrothermal system at Julcani, Peru: evidence from fluid inclusions and hydrogen and oxygen isotopes. Econ. Geol. 89, 1924–1938. https://doi.org/10.2113/gsecongeo.89.8.1924.

Dewey, J.F., Lamb, S.H., 1992. Active tectonics of the Andes. Tectonophysics 205, 79–95. https://doi.org/10.1016/0040-1951(92)90419-7.

Dipple, G.M., Ferry, J.M., 1992. Metasomatism and Fluid-flow in Ductile Fault zones. Contrib. Mineral. Petrol. 112, 149–164. https://doi.org/10.1007/BF00310451.

Durieux, C.G., Brown, A.C., 2007. Geological context, mineralization, and timing of the Juramento sediment-hosted stratiform copper–silver deposit, Salta district, northwestern Argentina. Mineral. Deposita 42, 879–899. https://doi.org/10.1007/s00126-007-0138-2.

Echavarria, L., Nelson, E., Humphrey, J., Chavez, J., Escobedo, L., Iriondo, A., 2006. Geologic evolution of the Caylloma epithermal vein district, Southern Perú. Econ. Geol. 101, 843–863. https://doi.org/10.2113/gsecongeo.101.4.843.

Filipovich, R., Chiodi, A., Báez, W., Ahumada, M.F., Invernizzi, C., Taviani, S., Giordano, G., 2022. Structural analysis and fluid geochemistry as tools to assess the potential of the Tocomar geothermal system, Central Puna (Argentina). Geothermics 98, 102297. https://doi.org/10.1016/j.geothermics.2021.102297.

Fischer, T.P., 2008. Fluxes of volatiles (H2O, CO2, N2, Cl, F) from arc volcanoes. Geochem. J. 42, 21–38. https://doi.org/10.2343/geochemj.42.21.

Flint, S., 1986. Sedimentary and diagenetic controls on red-bed ore genesis: the middle Tertiary San Bartolo copper deposit, Antofagasta province, Chile. Econ. Geol. 81, 761–778. https://doi.org/10.2113/gsecongeo.81.4.761.

Fontboté, L., Gorzawski, H., 1990. Genesis of the Mississippi valley-type Zn-Pb deposit of San Vicente, Central Peru; geologic and isotopic (Sr, O, C, S, Pb) evidence. Econ. Geol. 85, 1402–1437. https://doi.org/10.2113/gsecongeo.85.7.1402.

Fontboté, L., Amstutz, G.C., Cardozo, M., Cedillo, E., Frutos, J., 1990. In: Fontboté, L., Amstutz, G.C., Cardozo, M., Cedillo, E., Frutos, J. (Eds.), Stratabound Ore Deposits in the Andes. Springer Berlin Heidelberg, Berlin, Heidelberg. https://doi.org/10.1007/978-3-642-88282-1, 247 p.

Fullerton, K.M., et al., 2021. Effect of tectonic processes on biosphere–geosphere feedbacks across a convergent margin. Nat. Geosci. 14, 301–306. https://doi.org/10.1038/s41561-021-00725-0.

Garver, J.I., Reiners, P.W., Walker, L.J., Ramage, J.M., Perry, S.E., 2005. Implications for timing of Andean Uplift from thermal Resetting of Radiation-Damaged Zircon in the Cordillera Huayhuash, Northern Peru. J. Geol. 113, 117–138. https://doi.org/10.1086/427664.

Gat, J.R., 1996. Oxygen and hydrogen isotopes in the hydrologic cycle. Annu. Rev. Earth Planet. Sci. 24, 225–262. https://doi.org/10.1146/annurev.earth.24.1.225.

Gat, J.R., 1996. Oxygen and hydrogen isotopes in the hydrologic cycle. Annu. Rev. Earth Planet. Sci. 24 (1), 225–262. https://doi.org/10.1146/annurev.earth.24.1.225.

Gemmell, J.B., Zantop, H., Meinert, L.D., 1992. Genesis of the Aguilar zinc-lead-silver deposit, Argentina; contact metasomatic vs. sedimentary exhalative. Econ. Geol. 87, 2085–2112. https://doi.org/10.2113/gsecongeo.87.8.2085.

Giordano, G., Pinton, A., Cianfarra, P., Baez, W., Chiodi, A., Viramonte, J., Norini, G., Groppelli, G., 2013. Structural control on geothermal circulation in the Cerro Tuzgle-Tocomar geothermal volcanic area (Puna plateau, Argentina). J. Volcanol. Geotherm. Res. 249, 77–94. https://doi.org/10.1016/j.jvolgeores.2012.09.009.

Giovannelli, D., Barry, P.H., De Moor, J.M., Jessen, G.L., Schrenk, M.O., Lloyd, K.G., 2022. Sampling across large-scale geological gradients to study geosphere–biosphere interactions. Front. Microbiol. 13, 998133 https://doi.org/10.3389/fmicb.2022.998133.

Goff, F., Shevenell, L., Gardner, J.N., Vuataz, F.-D., Grigsby, C.O., 1988. The hydrothermal outflow plume of Valles Caldera, New Mexico, and a comparison with other outflow plumes. J. Geophys. Res. 93, 6041. https://doi.org/10.1029/jb093ib06p06041.

Gorzawski, H., Fontboté, L., Field, C.W., Tejada, R., 1990. Sulfur Isotope Studies in the Zinc-Lead Mine San Vicente, Central Peru: Stratabound Ore Deposits in the Andes, pp. 305–312. https://doi.org/10.1007/978-3-642-88282-1_22.

Hampel, A., 2002. The migration history of the Nazca Ridge along the Peruvian active margin: a re-evaluation. Earth Planet. Sci. Lett. 203, 665–679. https://doi.org/10.1016/S0012-821X(02)00859-2.

Hartmann, J., Moosdorf, N., 2012. The new global lithological map database GLiM: a representation of rock properties at the Earth surface. Geochem. Geophys. Geosyst. 13, 1–37. https://doi.org/10.1029/2012GC004370.

Hayes, G., 2018. A Comprehensive Subduction Zone Geometry Model: U.S. Geological Survey Data Release. https://doi.org/10.5066/F7PV6JNV.

Henley, R.W., Fischer, T.P., 2021. Sulfur sequestration and redox equilibria in volcanic gases. J. Volcanol. Geotherm. Res. 414, 107181 https://doi.org/10.1016/j.jvolgeores.2021.107181.

Henley, R.W., Fischer, T.P., 2021. Sulfur sequestration and redox equilibria in volcanic gases. J. Volcanol. Geotherm. Res. 414, 107181. https://doi.org/10.1016/j.jvolgeores.2021.107181.

Hiett, C.D., Newell, D.L., Jessup, M.J., 2021. He evidence for fluid transfer and continental hydration above a flat slab. Earth Planet. Sci. Lett. 556 https://doi.org/10.1016/j.epsl.2020.116722, p. 116722.

Hiett, C.D., Newell, D.L., Jessup, M.J., Grambling, T.A., Scott, B.E., Upin, H.E., 2022. Deep CO2 and N2 emissions from Peruvian hot springs: Stable isotopic constraints on volatile cycling in a flat-slab subduction zone. Chem. Geol. 595, 120787. https://doi.org/10.1016/j.chemgeo.2022.120787.

Hilton, D.R., Fischer, T.P., Marty, B., 2002. Noble Gases in Subduction Zones and Volatile Recycling.

Hoorn, C., et al., 2010. Amazonia Through Time: Andean Uplift, Climate Change, Landscape Evolution, and Biodiversity. Science 330, 927–931. https://doi.org/10.1126/science.1194585.

Horton, B.K., 2018a. Sedimentary record of Andean mountain building. Earth Sci. Rev. 178, 279–309. https://doi.org/10.1016/j.earscirev.2017.11.025.

Horton, B.K., 2018b. Tectonic regimes of the Central and Southern Andes: responses to variations in plate coupling during subduction. Tectonics 37, 402–429. https://doi.org/10.1002/2017TC004624.

Horton, B.K., Hampton, B.A., Waanders, G.L., 2001. Paleogene synorogenic sedimentation in the Altiplano plateau and implications for initial mountain building in the Central Andes. Bull. Geol. Soc. Am. 113, 1387–1400. https://doi.org/10.1130/0016-7606(2001)113<1387:PSSITA>2.0.CO;2.

Horton, B.K., Fuentes, F., Boll, A., Starck, D., Ramirez, S.G., Stockli, D.F., 2016. Andean stratigraphic record of the transition from backarc extension to orogenic shortening: a case study from the northern Neuquén Basin, Argentina. J. S. Am. Earth Sci. 71, 17–40. https://doi.org/10.1016/j.jsames.2016.06.003.

Jordan, T.E., Isacks, B.L., Allmendinger, R.W., Brewer, J.A., Ramos, V.A., Ando, C.J., 1983. Andean tectonics related to geometry of subducted Nazca plate. Geol. Soc. Am. Bull. 94, 341–361. https://doi.org/10.1130/0016-7606(1983)94<341:ATRTGO>2.0.CO;2.

Kagoshima, T., Sano, Y., Takahata, N., Maruoka, T., Fischer, T.P., Hattori, K., 2015. Sulphur geodynamic cycle. Sci. Rep. 5, 8330. https://doi.org/10.1038/srep08330.

Krouse, H.R., Grinenko, V.A. (Eds.), 1992. SCOPE 43. Stable Isotopes: Natural and Anthropogenic Sulphur in the Environment. John Wiley & Sons, New York, 440 p.

Krouse, H.R., Mayer, B., 2000. Sulphur and Oxygen Isotopes in Sulphate. In: Cook, P.G., Herczeg, A.L. (Eds.), Environmental Tracers in Subsurface Hydrology. Springer US, Boston, MA, pp. 195–231. https://doi.org/10.1007/978-1-4615-4557-6_7.

Labidi, J., Cartigny, P., Moreira, M., 2013. Non-chondritic Sulphur isotope composition of the terrestrial mantle. Nature 501, 208–211. https://doi.org/10.1038/nature12490.

Lages, J., Rizzo, A.L., Aiuppa, A., Samaniego, P., Le Pennec, Ceballos, J.A., Sandoval-Velasquez, A., 2021. Noble gas magmatic signature of the Andean Northern Volcanic Zone from fluid inclusions in minerals. Chemical Geology 559, 119966. https://doi.org/10.1016/j.chemgeo.2020.119966.

Laske, G., Masters, G., Ma, Z., Pasyanos, M., 2013. Update on CRUST 1.0 - A 1-degree global model of earth's crust. Geophys. Res. Abstr. 15.

Lee, C.T.A., Erdman, M., Yang, W., Ingram, L., Chin, E.J., DePaolo, D.J., 2018. Sulfur isotopic compositions of deep arc cumulates. Earth Planet. Sci. Lett. 500, 76–85. https://doi.org/10.1016/j.epsl.2018.08.017.

Lloyd, R.M., 1968. Oxygen isotope behavior in the Sulfate-Water System. J. Geophys. Res. 73, 6099–6110. https://doi.org/10.1029/JB073i018p06099.

Lloyd, R.M., 1968. Oxygen isotope behavior in the sulfate-water system. J. Geophys. Res. 73 (18), 6099–6110.

Maloney, K.T., Clarke, G.L., Klepeis, K.A., Quevedo, L., 2013. The late Jurassic to present evolution of the Andean margin: Drivers and the geological record. Tectonics 32, 1049–1065. https://doi.org/10.1002/tect.20067.

Manea, V.C., Manea, M., 2011. Flat-slab thermal structure and evolution beneath Central Mexico. Pure Appl. Geophys. 168, 1475–1487. https://doi.org/10.1007/s00024-010-0207-9.

Maza, S.N., Collo, G., Astini, R.A., Nieto, F., Nieto, J.M., 2014. Holocene ochreous lacustrine sediments within the Famatina Belt, NW Argentina: a natural case for fossil damming of an acid drainage system. J. S. Am. Earth Sci. 52, 149–165. https://doi.org/10.1016/j.jsames.2014.02.010.

Mizutani, Y., 1972. Isotopic composition and underground temperature of the Otake geothermal water, Kyushu, Japan. Geochem. J. 6, 67–73. https://doi.org/10.2343/geochemj.6.67.

Mizutani, Y., Rafter, T.A., 1969. Oxygen isotopic composition of sulphates. Part 4. Bacterial fractionation of oxygen Isotopes in the reduction of sulphate and in the oxidation of sulphur. N. Z. J. Sci. 12, 60–68 (Mar. 1969). https://www.osti.gov/biblio/4764537.

Nelson, S.T., 2000. A simple, practical methodology for routine VSMOW/SLAP normalization of water samples analyzed by continuous flow methods. Rapid Commun. Mass Spectrom. 14, 1044–1046. https://doi.org/10.1002/1097-0231(20000630)14:12<1044::AID-RCM987>3.0.CO;2-3.

Newell, D.L., Jessup, M.J., Hilton, D.R., Shaw, C.A., Hughes, C.A., 2015. Mantle-derived helium in hot springs of the Cordillera Blanca, Peru: implications for mantle-to-crust fluid transfer in a flat-slab subduction setting. Chem. Geol. https://doi.org/10.1016/j.chemgeo.2015.10.003.

O'Nions, R.K., Oxburgh, E.R., 1988. Helium, volatile fluxes and the development of continental crust. Earth Planet. Sci. Lett. 90, 331–347. https://doi.org/10.1016/0012-821X(88)90134-3.

Parada, M.A., Rivano, S., Sepulveda, P., Herve, M., Herve, F., Puig, A., Munizaga, F., Brook, M., Pankhurst, R., Snelling, N., 1988. Mesozoic and cenozoic plutonic development in the Andes of Central Chile (30°30′-32°30′S). J. S. Am. Earth Sci. 1, 249–260. https://doi.org/10.1016/0895-9811(88)90003-X.

Parnell, J., Carey, P.F., Bottrell, S.H., 1994. The occurrence of authigenic minerals in solid bitumens. J. Sediment. Res. A Sediment. Petrol. Proc. 64 A, 95–100. https://doi.org/10.1306/d4267d20-2b26-11d7-8648000102c1865d.

Petersen, U., 1965. Regional geology and major ore deposits of Central Peru. Econ. Geol. 60, 407–476. https://doi.org/10.2113/gsecongeo.60.3.407.

Petersen, U., Noble, D.C., Arenas, M.J., Goodell, P.C., 1977. Geology of the Julcani mining district, Peru. Econ. Geol. 72, 931–949. https://doi.org/10.2113/gsecongeo.72.6.931.

Poage, M.A., Chamberlain, C.P., 2001. Emperical relationships between elevation and the stable isotope composition of precipitation and surface waters: Considerations for studies of paleoelevation changes. Am. J. Sci. 301, 839–861. https://doi.org/10.2475/04.2007.01.

Polliand, M., Fontboté, L., Spangenberg, J., 1999. Tracing back sulfur isotope reequilibration due to contact metamorphism: a case study from the Perubar VMS deposit, Central Peru: Mineral deposits: processes to processing. In: 5th biennial SGA meeting, London, England, pp. 967–970.

Ramos, V.A., Folguera, A., 2009. Andean flat-slab subduction through time. Geol. Soc. Lond., Spec. Publ. 327, 31–54. https://doi.org/10.1144/SP327.3.

Ray, M.C., Hilton, D.R., Muñoz, J., Fischer, T.P., Shaw, A.M., 2009. The effects of volatile recycling, degassing and crustal contamination on the helium and carbon geochemistry of hydrothermal fluids from the Southern Volcanic Zone of Chile. Chem. Geol. 266, 38–49. https://doi.org/10.1016/j.chemgeo.2008.12.026.

Rielli, A., Tomkins, A.G., Nebel, O., Raveggi, M., Jeon, H., Martin, L., Ávila, J.N., 2018. Sulfur isotope and PGE systematics of metasomatised mantle wedge. Earth Planet. Sci. Lett. 497, 181–192. https://doi.org/10.1016/j.epsl.2018.06.012.

Ripley, E.M., Ohmoto, H., 1977. Mineralogic, sulfur isotope, and fluid inclusion studies of the stratabound copper deposits at the Raul Mine, Peru. Econ. Geol. 72, 1017–1041. https://doi.org/10.2113/gsecongeo.72.6.1017.

Rozanski, K., Araguas Araguas, L., 1995. Spatial and temporal variability of stable isotope composition of precipitation over the south American Continent. Bull. Inst. Franc. Etud. Andin. 24, 379–390.

Rusydi, A.F., 2018. Correlation between conductivity and total dissolved solid in various type of water: a review. IOP Conf. Ser. Earth Environ. Sci. 118. https://doi.org/10.1088/1755-1315/118/1/012019.

Rye, R.O., 1993. The evolution of magmatic fluids in the epithermal environment: the stable isotope perspective. Econ. Geol. 88, 733–753. https://doi.org/10.2113/gsecongeo.88.3.733.

Rye, R.O., 2005. A review of the stable-isotope geochemistry of sulfate minerals in selected igneous environments and related hydrothermal systems. Chem. Geol. 215, 5–36. https://doi.org/10.1016/j.chemgeo.2004.06.034.

Sakai, H., Marais, D.J.D., Ueda, A., Moore, J.G., 1984. Concentrations and isotope ratios of carbon, nitrogen and sulfur in ocean-floor basalts. Geochim. Cosmochim. Acta 48, 2433–2441. https://doi.org/10.1016/0016-7037(84)90295-3.

Sano, Y., Marty, B., 1995. Origin of carbon in fumarolic gas from island arcs. Chem. Geol. 119, 265–274. https://doi.org/10.1016/0009-2541(94)00097-R.

Scherrenberg, A.F., Jacay, J., Holcombe, R.J., Rosenbaum, G., 2012. Stratigraphic variations across the Marañón Fold-Thrust Belt, Peru: implications for the basin architecture of the West Peruvian Trough. J. S. Am. Earth Sci. 38, 147–158. https://doi.org/10.1016/j.jsames.2012.06.006.

Scherrenberg, A.F., Kohn, B.P., Holcombe, R.J., Rosenbaum, G., 2016. Thermotectonic history of the Marañón Fold–Thrust Belt, Peru: insights into mineralisation in an evolving orogen. Tectonophysics 667, 16–36. https://doi.org/10.1016/j.tecto.2015.11.007.

Schutfort, E.G., 2001. The Genesis of the San Vicente Lead Zinc Rhythmite Deposit, Peru a Petrologic, Geochemical, and Sulfur Isotope Study. Oregon State University, 150 p.
Scott, B.E., Newell, D.L., Jessup, M.J., Grambling, T.A., Shaw, C.A., 2020. Structural controls on crustal fluid circulation and hot spring geochemistry above a flat-slab subduction zone, Peru. Geochem. Geophys. Geosyst. https://doi.org/10.1029/2020gc008919, p. 0–2.
Sheppard, S.M., 1986. Characterization and isotopic variations in natural waters. Rev. Mineral. Geochem. 16 (1), 165–183.
Skirrow, R.G., Camacho, A., Lyons, P., Pieters, P.E., Sims, J.P., Stuart-Smith, P.G., Miró, R., 2000. Metallogeny of the southern Sierras Pampeanas, Argentina: geological, 40Ar-39Ar dating and stable isotope evidence for Devonian Au, Ag-Pb-Zn and W ore formation. Ore Geol. Rev. 17, 39–81. https://doi.org/10.1016/S0169-1368(00)00004-4.
Smith, J.A., Finkel, R.C., Farber, D.L., Rodbell, D.T., Seltzer, G.O., 2005. Moraine preservation and boulder erosion in the tropical Andes: interpreting old surface exposure ages in glaciated valleys. J. Quat. Sci. 20, 735–758. https://doi.org/10.1002/jqs.981.
Styron, R., Pagani, M., 2020. The GEM global active faults database. Earthquake Spectra 36, 160–180. https://doi.org/10.1177/8755293020944182.
Sundell, K.E., Saylor, J.E., Lapen, T.J., Styron, R.H., Villarreal, D.P., Usnayo, P., Cárdenas, J., 2018. Peruvian Altiplano stratigraphy highlights along-strike variability in foreland basin evolution of the Cenozoic Central Andes. Tectonics 37, 1876–1904. https://doi.org/10.1029/2017TC004775.
Suzuki, Y., Hayashi, K., 2019. Mineralogy, Fluid inclusions, and sulfur isotopes of the Huanzala Deposits, Peru: early Skarn and late polymetallic replacement style mineralizations. Resour. Geol. 69, 249–269. https://doi.org/10.1111/rge.12200.
Tassi, F., Aguilera, F., Darrah, T., Vaselli, O., Capaccioni, B., Poreda, R.J., Delgado Huertas, A., 2010. Fluid geochemistry of hydrothermal systems in the Arica-Parinacota, Tarapacá and Antofagasta regions (northern Chile). J. Volcanol. Geotherm. Res. 192, 1–15. https://doi.org/10.1016/j.jvolgeores.2010.02.006.
Tomkins, A.G., Evans, K.A., 2015. Separate zones of sulfate and sulfide release from subducted mafic oceanic crust. Earth Planet. Sci. Lett. 428, 73–83. https://doi.org/10.1016/j.epsl.2015.07.028.
Upin, H.E., Newell, D.L., Colman, D.R., Boyd, E.S., 2023. Tectonic settings influence the geochemical and microbial diversity of Peru hot springs. Commun. Earth Environ. 4, 112. https://doi.org/10.1038/s43247-023-00787-5.
USGS, 2006. National field manual for the collection of water-quality data. In: USGS (Ed.), U.S. Geological Survey Techniques of Water-Resources Investigations: Book 9, A1-A9. USGS.
Van Stempvoort, D.R., Krouse, H.R., 1993. Controls of δ18O in sulfate. In: Alpers, C.N., Blowes, D.W. (Eds.), Environmental Geochemistry of Sulfide Oxidation. American Chemical Society, Washington, D.C., pp. 446–480. https://doi.org/10.1021/bk-1994-0550.ch029
Varekamp, J., Ouimette, A., Kreulen, R., Delpino, D., Bermudez, A., 2001. Shallow magmatic degassing into the hydrothermal system of Copahue, Argentina. In: American Geophysical Union Spring Meeting 2001.
Vimeux, F., Ginot, P., Schwikowski, M., Vuille, M., Hoffmann, G., Thompson, L.G., Schotterer, U., 2009. Climate variability during the last 1000 years inferred from Andean ice cores: a review of methodology and recent results. Palaeogeogr. Palaeoclimatol. Palaeoecol. 281, 229–241. https://doi.org/10.1016/j.palaeo.2008.03.054.
Voute, F., Hagemann, S.G., Evans, N.J., Villanes, C., 2019. Sulfur isotopes, trace element, and textural analyses of pyrite, arsenopyrite and base metal sulfides associated with gold mineralization in the Pataz-Parcoy district, Peru: implication for paragenesis, fluid source, and gold deposition mechanisms. Mineral. Deposita 54, 1077–1100. https://doi.org/10.1007/s00126-018-0857-6.
Walters, J.B., Cruz-Uribe, A.M., Marschall, H.R., 2019. Isotopic compositions of sulfides in exhumed high-pressure Terranes: implications for sulfur cycling in subduction zones. Geochem. Geophys. Geosyst. 3347–3374. https://doi.org/10.1029/2019gc008374.
Walters, J.B., Cruz-Uribe, A.M., Marschall, H.R., 2020. Sulfur loss from subducted altered oceanic crust and implications for mantle oxidation. Geochem. Perspect. Lett. 36–41. https://doi.org/10.7185/geochemlet.2011.
Wilson, N.S.F., Zentilli, M., Spiro, B., 2003. A sulfur, carbon, oxygen, and strontium isotope study of the volcanic-hosted El Soldado Manto-type copper deposit, Chile: the essential role of bacteria and petroleum. Econ. Geol. 98, 163–174. https://doi.org/10.2113/gsecongeo.98.1.163.